# Observational evidence of new current sheets trailing coronal mass ejections

D. F. Webb,[1,2] J. Burkepile,[3] T. G. Forbes,[4] and P. Riley[5]

Received 6 March 2003; revised 6 August 2003; accepted 15 August 2003; published 16 December 2003.

[1] Field line reconnection in the wake of coronal mass ejections (CMEs) is a fundamental aspect of some magnetically driven eruptive flare/CME models, e.g., the standard reconnection model [cf. *Svestka and Cliver*, 1992]. This model features a growing hot loop arcade beneath a rising X-type neutral point that is connected to the retreating CME. In models invoking reconnection the rising CME and neutral point are connected by a stretched current sheet. Two recent models, *Lin and Forbes* [2000] and *Linker et al.* [2003], predict that an extended, long-lived current sheet must be formed for any physically plausible reconnection rate. Lin and Forbes derive estimates for heights or lengths of current sheets and the energy input as functions of time. In a previous observational study of SMM CMEs observed from 1984–1989 having candidate magnetic disconnection features, primarily transient concave-outward bright regions following the CME leading edge, we found that about half were followed by coaxial, bright rays suggestive of newly formed current sheets. The rays appeared relatively suddenly several hours after the main CME had left the field of view. In this paper we present the results of analysis of these structures, including their heights and lengths, widths, alignments, and motions, all as functions of time, and show that they are consistent with the existence of current sheets lasting for several hours and extending more than five solar radii into the outer corona. *INDEX TERMS:* 7513 Solar Physics, Astrophysics, and Astronomy: Coronal mass ejections; 7835 Space Plasma Physics: Magnetic reconnection; 7524 Solar Physics, Astrophysics, and Astronomy: Magnetic fields; 2111 Interplanetary Physics: Ejecta, driver gases, and magnetic clouds; *KEYWORDS:* coronal mass ejections, magnetic reconnection, solar flare theory

**Citation:** Webb, D. F., J. Burkepile, T. G. Forbes, and P. Riley, Observational evidence of new current sheets trailing coronal mass ejections, *J. Geophys. Res.*, *108*(A12), 1440, doi:10.1029/2003JA009923, 2003.

## 1. Introduction

### 1.1. Background

[2] The disconnection of magnetic field lines following coronal mass ejections (CMEs) is an important aspect of a class of eruptive flare models, and some kind of reconnection appears necessary to prevent the buildup of the net interplanetary magnetic flux. However, until the launch of the SOHO LASCO coronagraphs, the observation of events at the Sun providing evidence for disconnection, such as concave-outward structures, had been relatively rare. An early statistical survey of candidate features in the corona found that ~10% of all CMEs might be associated with disconnection structures [*Webb and Cliver*, 1995]. We have been involved in a general program to understand the physics of coronal restructuring during transient events. This overall study addresses some fundamental problems of coronal and heliospheric physics, including how field lines reconnect near the Sun, whether closed structures such as streamers and filaments typically reform following the ejection, and how consistent such observations are with the well-known lack of an observed increase of net flux in the heliosphere.

[3] Both observational and theoretical efforts to understand the development of CMEs have emphasized their initiation and early phases. Less effort, however, has been placed on understanding how the magnetic field evolves during the passage of the CME through the corona and how the structures opened during a CME evolve after the CME has passed into interplanetary space. In their summary of Skylab CMEs, *Gosling et al.* [1974] found that the CMEs seemed to retain their connection to the Sun for several days following the passage of the CME itself. The Skylab observations fostered the concept that CMEs are planar loop structures having "legs." However, many CMEs do not show a simple loop-like structure, and more detailed analyses suggest that CMEs have a more three-dimensional form [*Fisher and Munro*, 1984; *Webb*, 1988; *Hundhausen*, 1999].

[1]Institute for Scientific Research, Boston College, Chestnut Hill, Massachusetts, USA.
[2]Also at Air Force Research Laboratory, Space Vehicles Directorate, Hanscom Air Force Base, Massachusetts, USA.
[3]High Altitude Observatory/National Center for Atmospheric Research, Boulder, Colorado, USA.
[4]Institute for the Study of Earth, Oceans, and Space, University of New Hampshire, Durham, New Hampshire, USA.
[5]Science Applications International Corporation, San Diego, California, USA.

Copyright 2003 by the American Geophysical Union.
0148-0227/03/2003JA009923$09.00

[4] *Anzer and Poland* [1979] examined the changes in the "legs" of several Skylab CMEs, and concluded that these structures remain visible for more than a day, first dimming then brightening. *Kahler and Hundhausen* [1992] studied the late phase of 16 SMM CMEs and concluded that the bright structures following many CMEs are more plausibly interpreted as the tops of streamers which trace neutral sheets in the corona. Such streamers might have reformed following the reconnection of coronal fields during and after the CME. An excellent example of the reformation of a large helmet streamer observed by the Yohkoh SXT and the Mauna Loa Solar Observatory (MLSO) K-coronameter was reported by *Hiei et al.* [1993].

[5] A fundamental question concerning magnetic fields ejected from the Sun was discussed by *Gold* [1962] and subsequently applied to the late phase of CMEs by *Gosling* [1975] and *MacQueen* [1980]. They argued that the continual ejection of such magnetic structures from the Sun should cause the net magnetic flux permeating the interplanetary medium to increase indefinitely. For example, using counterstreaming electron events as a CME proxy, *McComas et al.* [1992; cf. *McComas*, 1995] found that, in the absence of any reconnection, CMEs would double the ecliptic field magnitude every 9 months. Since no such buildup is observed, the paradox could be resolved by having the extended CME field lines pinch off and disconnect, forming a set of closed loops near the solar surface and an outwardly propagating closed magnetic structure in the solar wind. Such a process would result in the CME magnetic flux being convected out of the heliosphere by the solar wind.

[6] Evidence for newly closed loops near the solar surface include X-ray long-decay events (LDEs), first studied during Skylab, which are associated with the later phase of both erupting filaments and CMEs. For instance, *Sheeley et al.* [1983] found that the probability of associating a CME with a soft X-ray flare increased linearly with the flare duration, reaching 100% for X-ray events of duration $\geq$6 hours. In X-ray images these events appear as large-scale loop arcades which grow in length and width with time and, as they cool, become visible in cooler lines. Mass appears to be advected upward from the chromosphere to fill the newly reconnected flux tubes [*Forbes et al.*, 1989]. SMM data indicate that the loops actually shrink with time as they cool [*Svestka et al.*, 1987]; the measured degree of shrinkage agrees with a simple potential field/current sheet model [*Forbes and Acton*, 1996]. Nonthermal emission detected at hard X-ray and radio wavelengths is also often observed just above the flare loops [*Magara et al.*, 1996]. This emission may arise from electrons accelerated below the CME at an X-type reconnection point or current sheet [*Cliver et al.*, 1986]. Another kind of coronal activity suggestive of disconnection is the moving type IV radio burst, interpreted as emission from accelerated particles trapped in a plasmoid. More recently, *Gopalswamy et al.* [1997] and *Bastian et al.* [2001] have found evidence of such structures moving outward from limb flares in Yohkoh-Nobeyama and LASCO-Nancay data, respectively.

[7] Yohkoh SXT observations clearly confirm that bright X-ray arcades, some with cusps on top, do form frequently in the low corona following the likely ejection of coronal mass. Is there evidence of the local opening of magnetic field lines? Yohkoh X-ray and ground-based radio images of limb events [e.g., *Shibata et al.*, 1995; *Hudson et al.*, 1996; *Gopalswamy et al.*, 1997; *Nitta and Akiyama*, 1999] suggest that some degree of rapid reconnection does in fact occur after some eruptive events, leading to the ejection of a plasmoid.

### 1.2. Observational Evidence of Disconnection in the Outer Corona

[8] Assuming that the coronal plasma outlines the field structures, one signature of the upper disconnection process in the mid corona might be an outward moving circular or ovoid "plasmoid" (at least as projected on the sky plane). Figure 1, adapted from *Webb and Cliver* [1995], shows an interpretative example of such a feature as it might appear near the Sun. This is a broad, circular CME wherein the contrast across a bright band (denser than ambient) below a darker than ambient interior void region suggests an outward-curved disconnected structure. Farther out in the corona or late in the event, only the base of such a feature might be visible. Another kind of feature (not shown) arises from a narrow plasmoid-type CME which occurs in and is ejected through a preexisting streamer [*Hundhausen*, 1999]. In both cases a thin neutral sheet and reforming streamer is left behind or below the departing CME. Any lower closed loop arcades usually lie beneath the occulting disk. Since the widths of streamers and CMEs range over many tens of degrees, we might expect similar widths of the disconnection structures. *Webb and Cliver* [1995] found that nearly 2/3 of what they called candidate disconnection features were circular or ovoid, and the remainder were partial outward arcs.

[9] However, coronagraph observations before LASCO implied that evidence of the large-scale disconnection of field lines was rarely observed near the Sun in the wake of CMEs. For example, no clear evidence of a disconnection event in coronagraph data was published until that featured by *Illing and Hundhausen* [1983], who interpreted an event observed in the 1980 SMM data as a disconnected CME. It appeared as a bright front concave-outward from the Sun moving outward through the corona several hours after the CME's leading edge. They interpreted the CME front as plasma on rising, closed field lines above an X-type reconnection region. Later a bright, narrow radial ray appeared, suggesting formation of a neutral or current sheet following the outward motion of the closed, detached magnetic structure [see also *Hundhausen*, 1999].

[10] Other concave-outward arcs or imbedded darker-than-ambient "void" features with outward-curved forms within CMEs have been detected in more recent coronagraph data, suggesting that disconnection events may not be as rare as previously thought. The limited observational evidence for disconnection events in the images from the Skylab, SMM and SOLWIND coronagraphs and even from ground-based solar eclipse observations was reviewed by *Webb and Cliver* [1995]. Their results indicated that transient coronal structures similar to the prototypical *Illing and Hundhausen* [1983] event could be detected in the mid corona following $\geq$10% of CMEs. However, with the more sensitive LASCO data, concave-outward structures have been detected in over 1/3 of all CMEs and nearly half of

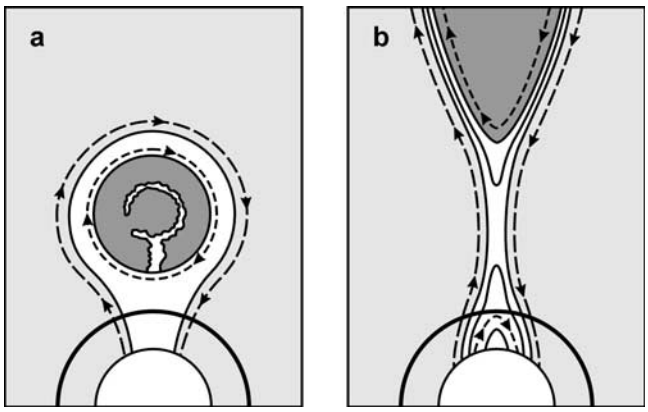


**Figure 1.** Schematic showing the evolution of a large, loop-like coronal mass ejection (CME) exhibiting signatures of magnetic disconnection in the low or middle corona, as it might appear within a few solar radii of the solar limb. Solid lines outline bright, denser plasma regions, and dashed lines suggest the direction of the constraining magnetic field lines. (a) An early phase, in which the contrast across a bright band below a dark interior void region suggests an outward-curved disconnected structure. This is a class 1 candidate disconnection event (CDE). A bright structure, often prominence material, may occasionally appear within the darker interior. (b) The base of such a feature as it might appear farther out in the corona or late in the event. Also drawn is the possible interconnection between the large-scale, rising structure and smaller-scale reconnecting loops near the surface. These lower structures might be obscured by the occulting disk of a coronagraph (curved line above the limb). Adapted from *Webb and Cliver* [1995].

those observed in 1997 [*St. Cyr et al.*, 2000]. Hereinafter, we refer to the CME-related events having such candidate magnetic disconnection features as candidate disconnection events (CDEs), with the proviso that such features possibly provide direct evidence of disconnection, but that this has not been proven.

[11] The association of erupting prominences with interplanetary magnetic clouds which can be modeled as flux ropes led *Chen et al.* [1997] to model a LASCO CME having a circular shape as an erupting flux rope with its feet tied to or extending below the surface. *Wood et al.* [1999], *Chen et al.* [2000], and others have discovered other LASCO events which can be modeled as erupting flux ropes, including several in which the circular structure can be observed very near the surface in EIT or LASCO C1 images. *Wu et al.* [1997, 1999] have used an MHD numerical simulation of helmet streamer and flux rope systems to model observed features of two LASCO CMEs. *Webb and Cliver* [1995] had noted that the most common type of disconnection feature in the older data was circular or ring shaped, but they did not interpret them as 3-D flux ropes. Although now usually so interpreted, it is uncertain if the concave-outward structures are indeed flux ropes either formed through reconnection or convected as preexisting structures into the solar wind, or of large-scale disconnected plasmoids, or all of these (see, e.g., the discussion by *Cliver and Hudson* [2002]).

[12] Several types of transient features suggesting closed magnetic structures have been identified in the interplanetary medium. These structures include disconnected fields (plasmoids), magnetic loops that remain connected to the Sun (“bottles”), or flux ropes which are a hybrid of these. *Bothmer and Schwenn* [1994], *Rust* [1994], *Bothmer and Rust* [1997], and others have associated some magnetic clouds with solar filament disappearances. Since both kinds of structures have been modeled as flux ropes and associated with CMEs, it is likely that many CMEs contain flux ropes. Bidirectional flows of solar heat flux electrons are interpreted as evidence that the loops are closed and, thus, good proxies for CMEs in the solar wind [e.g., *Gosling*, 1993]. Although *Gosling* [1993] and *Bothmer* [1999] have estimated that approximately 1/3 of all counterstreaming events are likely magnetic flux ropes, recent estimates suggest this ratio may be closer to 2/3 [e.g., *Marubashi*, 2000; *Webb*, 2002]. It remains difficult to understand the interplanetary field topology of a given CME structure, whether entirely closed (bottle or plasmoid), entirely open, or a mixture of closed and open [e.g., *Kahler and Reames*, 1991; *Gosling et al.*, 1995]. Such mixed or hybrid topologies are supported by *Shodhan et al.* [2000] who found that on average 41% of the fields within a sample of magnetic clouds were consistent with open topologies, with the clouds ranging from entirely open to partially open and closed to entirely closed (also see review by *Bothmer* [1999]).

### 1.3. Eruptive Flare Models and Current Sheet Development

[13] Theoretical efforts to understand the development of CMEs have been directed toward understanding the environment within which CMEs arise. Several basic approaches exist (see recent reviews by *Low* [1999], *Forbes* [2000], *Klimchuk* [2001], and *Wu et al.* [2000, 2001]). One approach is to initiate a CME with a pressure pulse that drives the plasma and its embedded field outward [*Dryer*, 1982; *Steinolfson and Hundhausen*, 1988]. This approach no longer seems viable because there is now good evidence that the amount of pressure required to open the field is not produced. Flare heating is too weak by at least an order of magnitude [*Low*, 1981; *Forbes et al.*, 1989], and it is often found to occur after onset [*Wagner et al.*, 1981; *Harrison*, 1986]. Numerical [*Wu and Guo*, 1997; *Wang et al.*, 1998a; *Wu et al.*, 2000, 2001] and analytical [*Gibson and Low*, 1998; *Chen*, 1989] models have been developed which include features such as the helmet streamer and cavity. However, these models do not include a mechanism which explains how slow changes in the photospheric magnetic field cause the coronal magnetic field to lose its equilibrium. Models which do incorporate such a mechanism [e.g., *Sturrock*, 1989; *van Ballegooijen and Martens*, 1989; *Forbes and Isenberg*, 1991; *Moore and Roumeliotis*, 1992; *Low and Smith*, 1993; *Mikic and Linker*, 1994, 1997; *Wolfson and Dlamini*, 1997; *Antiochos et al.*, 1999; *Amari et al.*, 2000; *Sturrock et al.*, 2001] involve determining the stability, or existence, of sequences of equilibria generated by physically plausible changes in the photospheric magnetic field [*Low*, 1984, 1990].

[14] Most CME initiation models are storage models [e.g., *Forbes*, 2000; *Klimchuk*, 2001]. In these models

stresses build up gradually in the corona until a critical point is reached where a stable equilibrium is no longer possible. At this time the field erupts, releasing the magnetic energy associated with coronal currents. Storage models can be divided into those based on force-free volume currents and those based on current sheets. Both involve reconnection of the magnetic fields which are opened by the CME, but the latter class of models also include reconnection in a current sheet which exists prior to onset. After the field lines are opened, they reconnect to form a magnetic arcade of cusp-shaped loops, and a helical flux rope disconnected from the Sun except at its ends. The arcade and flux rope are connected at an X-type reconnection point, which rises as the system evolves. Observations of eruptive events since Skylab have provided support for this class of models. Until recently such models have been only 2D or 2.5D. In 3D models a flux rope tied only at its ends can be ejected with or without reconnection, however shear-driven reconnection may still be important for formation of the original flux rope [e.g., *Gosling*, 1993].

[15] Resistive MHD models of CMEs involve a sudden release of magnetic energy stored and built up in the corona. For example, *Mikic and Linker* [1994] describe the dynamical evolution of arcades due to photospheric shear flows finding that, when a critical shear value is exceeded, and the resistivity increased, the rising arcade field lines open rapidly to form a current sheet. Rapid reconnection at this sheet leads to fast flows, dissipation of magnetic energy and ejection of a plasmoid or CME. Simulations [e.g., *Forbes*, 1990; *Forbes and Priest*, 1995] suggest that reconnection in the current sheet below a flux rope might occur very rapidly, ejecting the rope. The rising flux rope creates flows which tend to stretch the current sheet until it becomes thin enough to undergo rapid reconnection. This basic concept was developed by *van Tend and Kuperus* [1978] and was also used by *Martens and Kuin* [1989], *Magara et al.* [1997], *Chen and Shibata* [2000], and others. The main driving force in these models is a catastrophic loss of MHD equilibrium operating on Alfven timescales (see the review by *Forbes* [2000]). *Forbes and Priest* [1995] found that following loss of equilibrium, the flux rope will jump to a higher altitude creating a vertical current sheet, as shown in Figure 2. To produce an ejection in the 2-D or 2.5-D models, reconnection in the current sheet must proceed rapidly enough to allow the rope to escape. Specifically, *Lin and Forbes* [2000] found that the inflow Alfven Mach number at the reconnection site must be greater than 0.05 for high-speed (>1000 km $s^{-1}$) CMEs. In 3-D models it may be possible for the flux rope to escape no matter how slow the rate of reconnection is. *Sturrock et al.* [2001] have argued that the field lines overlying the flux rope may slip to the side without becoming stretched, and if this occurs, then reconnection is not needed to cut the field lines holding the flux rope down.

[16] *Hudson and Khan* [1996] and others have pointed out the lack of supporting observations for the flows required by the reconnection model. However, several observations have recently been made of flows and heating that seem directly related to reconnection in current sheets or an *X* point [*Yokoyama et al.*, 2001; *McKenzie and Hudson*, 1999; *Tsuneta et al.*, 1997]. *Yokoyama et al.* [2001] used Yohkoh and EIT imagery of an eruptive flare and CME on 18 March 1999 to derive an inflow speed toward the presumed *X* point of 5 km $s^{-1}$. In similar LASCO and UVCS observations of two CMEs on 23 March 1998 and 8 January 2002, *Ciaravella et al.* [2002] and *Ko et al.* [2003] detected narrow structures radially beneath the departing CMEs which were hot (~6–8 MK) and dense ($10^8$ $cm^{-3}$). They find that the physical and dynamical properties of these structures are consistent with their being current sheets. Finally, *McKenzie and Hudson* [1999] and *McKenzie* [2000] have reported observations of dark downflows in several Yohkoh soft X rays above bright limb arcades following CMEs. These downflows could be associated with CME material which fails to achieve escape velocity or with the shrinkage of magnetic field lines that have reconnected and are forming the arcade [*Forbes and Acton*, 1996].

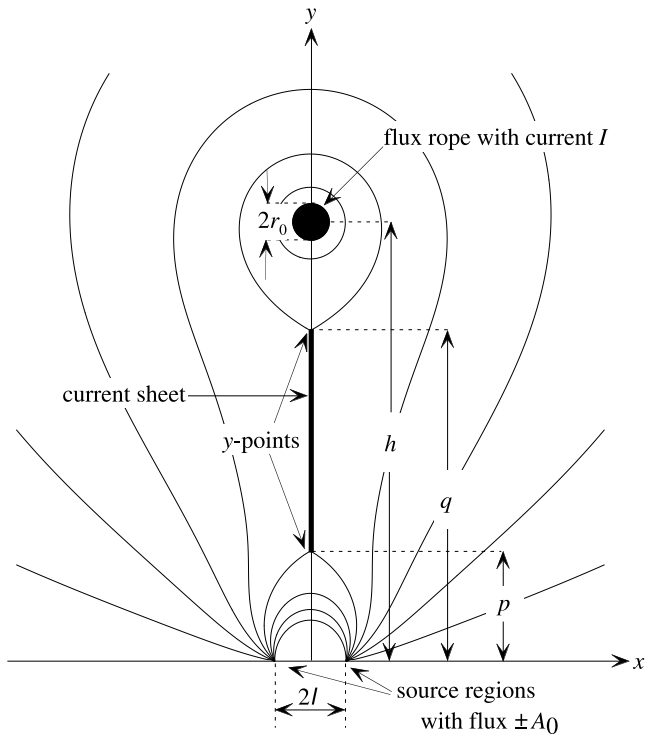


**Figure 2.** Diagram of the erupting flux rope model of *Lin and Forbes* [2000]. The flux rope is driven upward because of a loss of equilibrium due to two point sources at the base moving toward each other. Reconnection leads to a vertical current sheet, which, at any given time, extends from the Y-shaped points at the top of a growing arcade, $y = p$, to the base of the flux rope, $y = q$.

[17] In this paper we describe a set of observations made by the NCAR High Altitude Observatory (HAO) C/P coronagraph on SMM and the MLSO K-coronameter in Hawaii of bright, coaxial, narrow transient rays which formed relatively suddenly in the wake of CMEs, then faded or disappeared hours later. In light of the results discussed above, it seems plausible that these rays are associated with current sheets forming as a result of reconnection behind the main CME. We present the results of our analysis of these structures which includes their heights, lengths, widths, alignments, and motions, all as

functions of time. We then compare these results with two reconnection models which provide specific predictions for the current sheet evolution, the *Lin and Forbes* [2000] and *Linker et al.* [2003] models. *Webb et al.* [2001] gave a report on the preliminary results of this study. In the next section we discuss our method and show some examples. In section 3 we present the results of the measurements of the rays, and in section 4 we compare these with the models. In the last section we summarize and discuss the results.

## 2. Method and Examples

[18] Until the launch of SOHO, observations providing evidence for reconnection/disconnection of magnetic field lines following CMEs had been infrequent. In the statistical survey of *Webb and Cliver* [1995] they concluded that $\geq$10% of all CMEs might be associated with CDEs, primarily transient, concave-outward bright regions following the CME leading edge. However, the cadences of the data sets used in that survey were not optimum, leading two of us, DFW and JB, to perform a more comprehensive survey and analysis of CMEs observed by the HAO SMM coronagraph from 1984–1989. However, those results tended to confirm the earlier surveys and were never published. Because these SMM CDEs form the original data set from which the rays of this study were selected and for comparison with the earlier CDE studies, we present a summary of the analysis results of the SMM CMEs having CDEs in Appendix A.

[19] Our survey was initially influenced by the study of *Kahler and Hundhausen* [1992] who surveyed the SMM data from 1984–1987 during the minimum between solar cycles 21 and 22. Their goal was to understand the bright radial features which follow CMEs and that had been interpreted as "legs" during the Skylab era. They examined the late phase of 16 SMM CMEs and concluded that the bright structures following many CMEs were more plausibly interpreted as the tops of streamers which delineate current sheets in the corona. Such streamers might have reformed following the reconnection of coronal fields during and after the CME.

[20] For the general SMM CME study described in Appendix A, we used the final version of the *Burkepile and St. Cyr* [1993] catalog of SMM CMEs as a guide. During each CME this catalog notes if there were concave-outward features that were V-shaped or U-shaped. We examined the CMEs having these features as well as some noted from other studies, and found $\sim$60 CME-CDE events observed by the SMM coronagraph from 1984 to mid-November 1989. These events are described in Appendix A.

[21] *Kahler and Hundhausen* [1992] concluded that the new streamers following CMEs became evident about 12 hours after observation of the CME. In the slow *Illing and Hundhausen* [1983] event, the late ray appeared 15–20 hours later. Thus to adequately search the SMM CDE data for late rays, we limited the search to those CDEs which had good SMM coverage before, during and within at least 12 hours following observations of the CME leading edge. Our criteria used to search for rays suggestive of newly formed current sheets included newly forming, relatively bright, narrow rays which were approximately coaxial with and followed the CDE. 45 of the 59 CDEs (see Appendix A) met the time coverage criterion, and over half (26 or 58%) of these events were followed by candidate, new rays. Surprisingly, we found that the rays typically appeared relatively suddenly several hours after the CME leading edge had left the field of view.

[22] We analyzed these 26 events to test the hypothesis that the rays trace current sheets in the mid corona that arise because of reconnection in the wake of CMEs and their associated flux ropes. Our measurements of these structures included their heights and lengths, widths, and brightness variations all as functions of time. We then compared these results with the *Lin and Forbes* [2000] and *Linker et al.* [2003] models.

[23] Table 1 presents key information on the 26 SMM CMEs which had CDEs followed by late rays. There were no events in 1985 that had conclusive evidence of late rays. Column 1 is a unique number given to each CDE and its accompanying ray. The next seven columns refer to observations of the CDE, the next three columns to the associated CME, and column 12 to how any associated streamer was effected. For the CDE, the date and time of its first observation are given, followed by its width, speed and apparent morphology, and whether the late ray appeared to connect to the CDE or trailing edge of the CME within the SMM field of view, and finally in column 8 an estimate of the quality of the SMM imagery. For the associated CME, the first observed time, angular width and speed of its leading edge are given in columns 9–11.

[24] The mean width of the CDEs with rays was 24° (range 8°–55°) and their average outward speed was 130 km $s^{-1}$ (range 35–417 km $s^{-1}$). These values are very similar to those of all the SMM CDEs (see Appendix A, Tables A2 and A3). The average width and leading edge speed of the CMEs associated with the CDEs with rays were 44° (range 28°–65°) and 218.5 km $s^{-1}$ (range 16–577 km $s^{-1}$), resp. These values are the same as and less than, resp., those of all the CMEs with trailing CDEs (see Appendix A, Tables A2 and A3). Thus the results for the SMM CMEs and CDEs confirm those of *Webb and Cliver* [1995] that the CDEs are significantly narrower and slower than their accompanying CMEs. The widths and speeds of the CMEs themselves were only slightly lower than those of typical SMM CMEs, except for those CMEs with both CDEs and rays. The average CME speeds of the latter were slower, although there was a large range with three CMEs exceeding 500 km $s^{-1}$.

[25] Column 6 lists the morphological shapes of the CDEs with rays. The most common type was U-shaped (10) followed by equal numbers of V- and Light-bulb shapes (six each); the other five were uncertain or could be categorized as either U-shaped or V-shaped. Again, these distributions mimic those of the full sample of SMM CDEs (see Appendix A). We examined the preexisting coronal structures within which the CMEs seemed to occur to see if and how they were affected by the CME. In general, we agreed with the terminology and assessments of each event by *Burkepile and St. Cyr* [1993]. Our evaluations are listed in column 12. We note that 21 of the 26 events (81%) significantly disrupted an associated streamer, and in most of these (14) the streamer was completely blown out. In the

**Table 1.** SMM Candidate Disconnection Events With Late Rays

| | | Candidate Disconnection Event | | | | | | Coronal Mass Ejection | | | |
|---|---|---|---|---|---|---|---|---|---|---|---|
| No. | Date | First Observation, UT | Span, deg | Speed, km $s^{-1}$ | Shape | +Ray? | Quality[a] | First Observation, UT | Span, deg | Speed, km $s^{-1}$ | Streamer |
| 1 | 2 Oct. 1984 | 2118 | 39 | 39 | V | Y | G | 1420 | 39[b] | 65 | no str.? |
| 2 | 18 Oct. 1984 | 0936 | 24 | | LB | N | F | 0355 | 47 | 194 | disrupted |
| 3[c] | 14 Nov. 1984 | 0815 | 23 | 57 | V | N | G | 13, 2249 | 48 | 31? | blowout |
| 4 | 10 Dec. 1984 | 0107 | 28 | 106 | LB | Y? | G | 9, 2330 | 28[b] | 220 | disrupted |
| 5 | 13 Feb. 1986 | <1851 | 20 | 417 | U | N | F | 0327 | | | (poor data) |
| 6 | 26 Oct. 1986 | 1259 | 24 | 35 | LB | N | G | ~0345 | 30 | 70 | blowout |
| 7 | 24 May 1987 | 1323 | 15 | 178 | V | N | F, P | 1014 | 50 | 143 | (too faint) |
| 8 | 24 May 1987 | 1356 | 15 | | U | Y? | F | 1323 | | | (too faint) |
| 9 | 24 Sept. 1987 | 2144 | 40 | 146 | LB | Y? | G | 1734 | 42 | 134 | disrupted |
| 10 | 25 Sept. 1987 | 2300 | 26 | 77 | U | N | F | 1817 | 46 | | disrupted |
| 11 | 7 Nov. 1987 | 1818 | 20 | 145 | U | N | G | 1745 | 47 | 270 | blowout |
| 12 | 12 Feb. 1988 | 0926 | 24 | | ? | N | F, P | 0707 | 44 | 308 | disrupted |
| 13 | 6 May 1988 | 0144 | ~50 | | V? | Y | F | 0010 | 60 | 521 | blowout |
| 14 | 6 May 1988 | 1700 | 30 | 138 | LB | Y? | G | 1218 | 32 | 171 | blowout |
| 15 | 23 Aug. 1988 | 1841? | ? | | ? | Y | F | 1651 | 65 | 577 | blowout |
| 16 | 24 Aug. 1988 | 0032 | 11 | | VorU | Y | F | 23, 2307? | ? | | (cannot tell) |
| 17 | 14 Sept. 1988 | 1537 | 55 | | LB | N | G | 1346 | 55[b] | 506 | blowout |
| 18 | 15 Sept. 1988 | 0951 | 21 | 148 | U? | Y | G | 14, 2335 | 21[b] | ≥16 | blowout |
| 19 | 16 Nov. 1988 | 0341 | 14; 20 | 47; 50 | 2 Us | N | G | 15, 1936 | 45 | 188 | blowout |
| 20 | 21 Nov. 1988 | 2330 | 19 | 146 | VorU | N | F | 2030 | 60 | 202 | blowout |
| 21 | 19 Dec. 1988 | 1355 | 15 | 96 | V | N | F, P | 0433 | 55 | 34 | disrupted |
| 22 | 24 Dec. 1988 | 1934 | 14 | 366 | U | N | F | 1320 | 55? | 514 | blowout |
| 23 | 8 Jan. 1989 | 0343 | 28 | | VorU | N | P | 0310 | 30 | | (too faint) |
| 24 | 18 Feb. 1989 | 0423 | 21 | 59 | U | N | G | 0116 | 39 | | blowout |
| 25 | 1 June 1989 | 1551 | 18 | | U | N | F | ~0800 | ~13 | | disrupted |
| 26 | 6 Oct. 1989 | 1322 | 8 | 82 | V | N | G | ~0331 | 43 | 96 | blowout |

[a]G, good; F, fair; P, poor.
[b]The spans of the candidate disconnection event (CDE) and the coronal mass ejection (CME) are the same because the CME is circular.
[c]See *Kahler and Hundhausen* [1992, Figure 2].

other five cases, there was no clear preexisting streamer, the data was poor or the structures were too faint to evaluate. This rate of disruption is somewhat higher than that of the full sample of SMM CDEs (see Appendix A) in which 61% of the streamers were disrupted.

[26] We show two examples of SMM CMEs with CDEs followed by trailing, transient ray-like structures. Figure 3 shows the evolution of the 20–21 November 1988 CME in the southwest (Table 1, number 20). It was typical of the events in several respects. The preexisting streamer swelled and brightened, then blew out as the CME. The CME had a broad, outer loop enveloping a dark cavity, within which appeared a bright, circular core. This core expanded outward, revealing a V-shaped "back" with a stalk extending below the occulter. Many hours later a very bright, narrow ray suddenly appeared a few degrees south of the axis of the previous CME and CDE. As shown in the bottom right panels, the ray was also visible later in the day in the MLSO image where it appeared as an extension of a newly formed helmet streamer.

[27] The height-time plots of these features are shown in Figure 4 and illustrate our method for measuring the lengths of the rays and their lifetimes. The CME front is best fit by a constant acceleration with a final velocity of 202 km $s^{-1}$. The back or base of the V-shaped core (the CDE) could only be measured on five images; we fit the height-time profile of this structure with a constant velocity of 146 km $s^{-1}$ and extrapolated this curve to the time when the ray was last clearly visible. The times of the images on which the ray position angles and widths were measured are denoted by the large asterisks and the vertical dashed lines. The lifetime of the ray is defined as the time interval between when it was first and last visible as a separate feature. If we make the important assumption that the ray is a current sheet that always connects the base of a rising flux rope with the top of a growing surface arcade, then its length will be equivalent to the increasing heights denoted by the dashed lines. (Note, however, that with the SMM data we could not actually observe the rays beyond a height of ~6 $R_S$.) This assumed length is considered equivalent to the length, $q$, in the Lin and Forbes model (Figure 2). Although ideally we seek to measure the length of the current sheet itself, $q - p$, in most cases no arcade or streamer base appeared above the edge of the SMM occulting disk. Also, in some of the cases an acceleration curve was the best fit to the CDE points, which would increase the estimated ray lengths compared to a constant velocity fit. Thus the lengths we measure in these events are probably lower limits to the actual current sheet lengths. In the November 1988 event we observed and measured the height of the helmet base in MLSO observations late in the event.

[28] Figure 5 shows the development of another blowout CME in the southeast on 14–15 September 1988 (Table 1, number 18), and Figure 6 the height-time plot of the CDE and the ray measurement times. The east limb was active during this period. In the same image showing the preexisting streamer (14 September, 1845 UT), a late ray from a prior CME-CDE (Table 1, number 17) appears in the northeast. In event number 18, the leading edge of the CME was diffuse and could not be measured. A concave-outward, U-shaped feature moved out well behind the front.

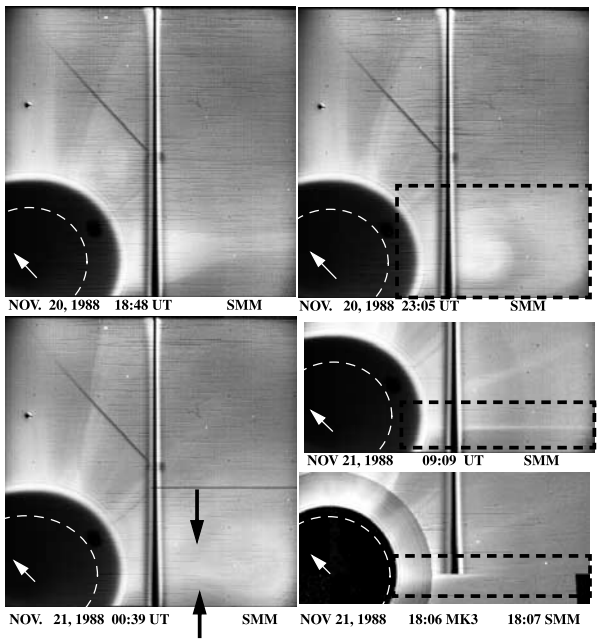


**Figure 3.** Evolution of the 20–21 November 1988 SMM CME in the southwest. The preexisting streamer swelled and brightened (20, 1848 UT), then blew out as the CME. The CME had a broad outer loop enveloping a dark cavity, within which appeared a bright, circular core (20, 2305 UT). The core later revealed a V-shaped "back" with a stalk extending below the occulter (21, 0039 UT). Hours later, a very bright, narrow ray suddenly appeared a few degrees south of the axis of the previous CME and CDE (21, 0909 UT). Below this panel is a Mauna Loa Solar Observatory (MLSO) image later on this day superposed within the SMM occulting disk, showing that the ray was part of a newly formed helmet streamer. The curved dashed lines indicate the limb of the Sun, and the arrows point to solar north. The vertical and diagonal lines and the small circular feature in each panel are detector artifacts.

In this case the ray, or its broader, fainter precursor, was present in the same field of view as the CDE. This ray, or a new one became more sharply delineated a few hours later, along with another ray 8° farther south. As *Kahler and Hundhausen* [1992] found, multiple ray-like structures are common following CME fronts; however, our focus was on any new, bright, narrow rays that appeared and were coaxial with the CDE, if not the CME itself. As shown in Figure 5, the ray was also visible in MLSO images of the low corona late on 15 September, but it is unclear whether the streamer at its base was newly forming. The height-time plot of Figure 6 shows that the CDE could be fit with a constant velocity of 148 km $s^{-1}$.

## 3. Results

[29] In this section we present the results of analysis of the transient ray structures, specifically their widths, alignments and motions, and their heights or lengths and lifetimes, all as functions of time. We also discuss their associations with flares and prominences near the surface using MLSO observations. Then, in section 4 we will compare the ray measurements with two CME models involving reconnection that make observable predictions, the Lin and Forbes and Linker et al. models. The parameters of the CDEs and rays that we derive and that are used in these comparisons are their height-time development and lifetimes.

### 3.1. Widths, Alignments, and Motions of the Rays

[30] The width and height measurements were performed by JB at HAO using cursor techniques on sequential computer displays of the images. The accuracy of the width measurements is ~0.2 and of the height measurements is ~0.1 $R_S$, but some of the rays were easier to measure than others. Alignments and motions of the rays were readily detected on movie sequences of each event.

[31] Table 2 presents these measurements for 27 rays observed during the 26 CME-CDE events of Table 1 (in the last event in 1989 two rays appeared and were measured separately). Table 3 summarizes the statistical results. The first five columns of Table 2 list the date, first measurement time of the ray, and the central position angles (counterclockwise from solar north through the east) of the CME front [from *Burkepile and St. Cyr*, 1993], the CDE and the ray. Columns 6 and 7 list the angular distance between the central axis of the CME and the ray and, if they were not coaxial, whether the ray was equatorward (E) or poleward (P) of the CME. Column 8 lists whether or not the ray was essentially coaxially aligned with the central axis of the CDE. (The CME's central axis is defined by its central position angle.) Columns 9 and 10 indicate whether or not

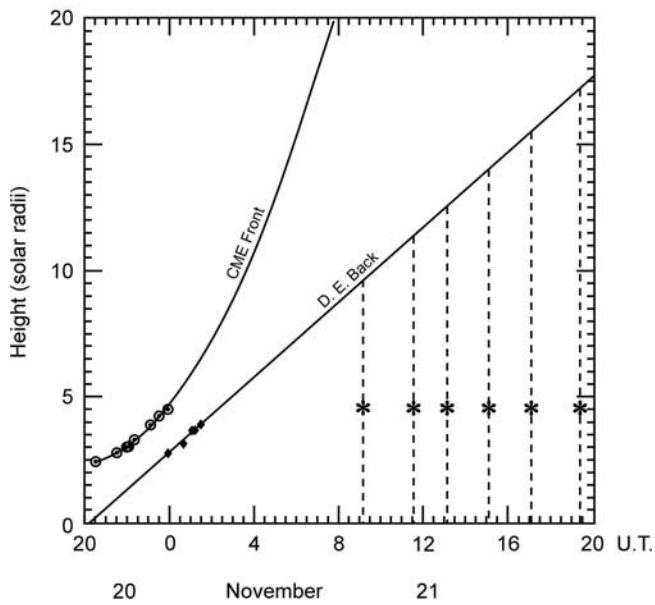


**Figure 4.** Height-time plots of the 20–21 November 1988 CME (circles) and CDE (squares) shown in Figure 3. The CME front points are best fit by a constant acceleration, whereas the back or base of the V-shaped core (the CDE) is fit with a constant velocity curve. This line is extrapolated to the time when the ray was last clearly visible. The times of the images on which the ray position angles and widths were measured are denoted by the large asterisks and the vertical dashed lines.

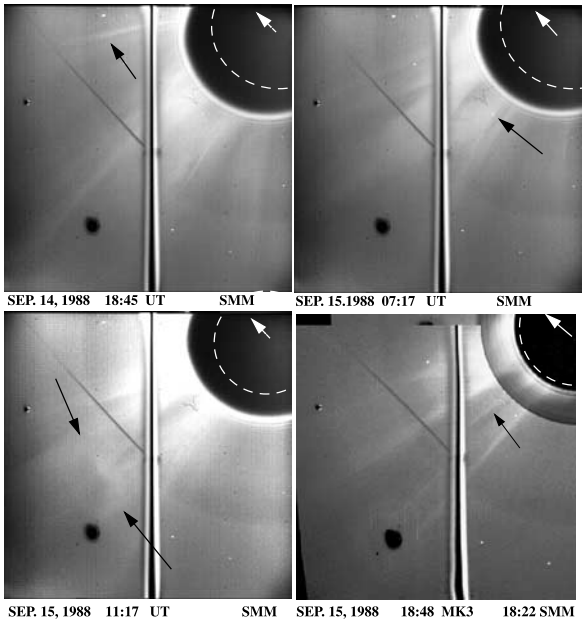


**Figure 5.** Development of a blowout CME in the southeast on 14–15 September 1988. In the image showing the preexisting streamer (14, 1845 UT) a late ray from a prior CME-CDE (arrow) appears in the northeast. In the later event a dark cavity (arrow; 15 September, 0717 UT) moved slowly outward behind the diffuse front. This was followed by a concave-outward, U-shaped feature (arrows; 15 September, 1117 UT), with the ray, or its broader, fainter precursor, present in the same field of view as the CDE. This same ray, or a new one, became more sharply delineated a few hours later (arrow; 15 September, 1822/1848 UT), along with another 8° farther south. The hair-like structure at the limb, the dark, circular spot, and the vertical and diagonal lines in each panel are detector artifacts.

the ray extended outward nonradially and, if so, whether it was tilted equatorward (E) or poleward (P). Columns 11 and 12 list whether the ray exhibited lateral motion during its lifetime and, if so, whether that motion was in the equatorward (E) or poleward (P) direction. In column 13 is the measured width of the ray, with the height that it was measured in parentheses. Columns 14–17 list timing data related to the lifetimes of the rays, and the last two columns denote the lengths of the rays derived from the height-time data. The timings and lengths are discussed later.

[32] Table 3 is a summary of the results from Table 2. We found that the mean width of the rays was 2.5° with a range of 1.3°–5.1°. For consistency, all the rays were measured at the lowest height in the coronagraph image but above the vignetting effects from the occulter. This mean height was 1.2 $R_L$ with a range of 0.8–3.2 $R_L$. (The unit, $R_L$, which we use hereafter, denotes the measured height above the solar limb in solar radii, $R_S$.) The mean of the angular offset between the axes of the CMEs and their associated rays was 9.1° with a range of 1°–24°, and most of the rays (74%) lay poleward of the CME axis. Most of the rays (78%) were coaxial with their accompanying concave-outward structure (this is partly a selection effect since the rays were required to be approximately coaxial with their associated CDE). However, the majority of the rays (76%) extended outward nonradially and most of these were tilted equatorward (79%). In terms of any lateral motion exhibited during the ray's lifetime, 10 of the rays displayed motion, 13 did not, and 4 were indeterminate. The ray's motions were about equally split between equatorward (six) and poleward (four). It is interesting that the ray motion seemed solar-cycle-dependent in that most of the moving rays occurred during the minimum and rising phases of the cycle, 1984 through mid-1987, and most of the stationary rays were during the maximum phase from late 1988 through 1989. This pattern seems consistent with the tendency of coronal streamers [e.g., *Hundhausen*, 1977] and CMEs [*Hildner*, 1977; *MacQueen et al.*, 1986] to be nonradial in the equatorward direction during solar minimum and mostly radial during maximum. However, the overall alignment of the rays was equatorward and did not exhibit a solar-cycle effect.

### 3.2. Lifetimes and Lengths of the Rays

[33] We can use the time intervals between the appearances of certain features to estimate the durations or lifetimes of the features, in particular the transient rays. We consider four time markers for each of the 27 events. These are (1) the onset time of the CME, i.e., the time of the SMM image on which it was first detected; (2) the time of the image when the back of the CDE is last visible; (3) the time of the image on which the ray is first visible; and (4) the time of the image when the ray is last visible. We use the term "visible" to mean when the feature is first or last

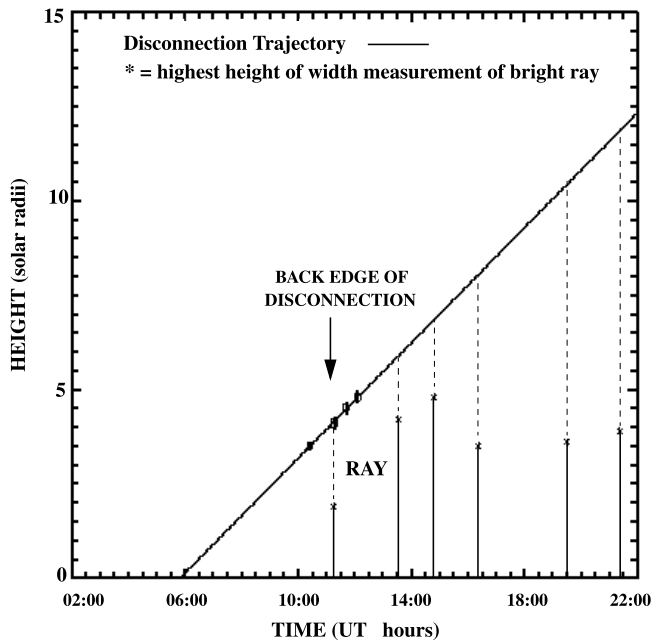


**Figure 6.** Height-time plot of the 14–15 September 1988 CDE shown in Figure 5. The four CDE measurements are best fit with a constant velocity curve, which is extrapolated to ~12 $R_S$ at the time of the last ray measurement. The solid vertical lines denote the times and the asterisks the highest heights at which the ray positions and widths were measured; the dashed lines extend these points to the extrapolated heights of the back of the CDE.

**Table 2.** Measurement Results of Late Rays

| | | Pos. Angle, deg | | | | | Alignment Motion | | | | | | Durations, hours | | | | Ray Length, $R_S$ | |
|---|---|---|---|---|---|---|---|---|---|---|---|---|---|---|---|---|---|---|
| Date | Time, UT | CME | CDE | Ray | CME Ray Dist., deg | CME Ray Dir. | Coax. | Nonrad. | Non-rad. Dir. | Ray Mot. | Ray Mot. Dir. | Ray Width (Height), deg ($R_S$) | CME-CDE | CDE Ray Str. | CDE Ray End | Life-time | Life | Meas. |
| 3 Oct. 1984 | 0604 | 107 | 117 | 117 | 10 | P | yes | yes | E | yes | P | 2.9 (1.8) | 10:15 | 21:20 | >24 | >2:40 | | |
| 18 Oct. 1984 | 1245 | 68 | 61 | 57 | 9 | P | no? | yes | E | yes | E | 1.3 (2.5) | 8:10 | 2:25 | ~10 | ~7:35 | 2.6–6.5 | 3.55–6.15 |
| 14 Nov. 1984 | 1742 | 101 | 109 | 108 | 6.5 | P | yes | yes | E | | | 1.4 (1.8) | ≥14:10 | 4:40 | >9 | >4:20 | 2.8–>5.5 | 3.65–4.6 |
| 10 Dec. 1984 | 0725 | 77 | 67 | 65 | 12 | P | yes? | yes | E | yes | E | 2.3 (1.8) | 4:45 | ≥1:35 | 8 | 6:25 | 3.5–7.8 | 5.25–5.6 |
| 13 Feb. 1986 | 2200 | 265 | 255 | 261 | 3 | P | no | yes | E | yes? | P | 2.9 (1.8) | ? | 3:10 | ≥7:50 | ≥4:30 | 4.4–>21.4 | 8.4–11.75 |
| 27 Oct. 1986 | 0453 | 100 | 93 | 97 | 3 | E | no? | | | | | 3.2 (1.8) | 20:30? | 3:30 | 13 | 9:30 | 2.9–>5.6 | 3.8–4.9 |
| 24 May 1987 | 1805 | 305 | 308 | 319 | 14 | P | no | yes? | E | yes | E | 1.8 (2.2) | 6:15 | 2:30 | new str. | | 3.3–? | 5.65–7.65 |
| 24 May 1987 | 1505 | 244 | 244 | 243 | 1 | | yes | no | | yes | E | 2.1 (2.6) | 1:40 | 7:45 | 9:15 | 1:30 | | |
| 25 Sept. 1987 | 0227 | 91 | 82 | 83 | 8 | P | yes | yes | P | no | | 1.9 (2.6) | 7:15 | ~1:00 | ~11 | ~10 | 2.45–11.2 | 4.3–10.0 |
| 26 Sept. 1987 | 1341 | 267 | 260 | 251 | 16 | P | yes? | yes | E | no | | 1.8 (2.5) | 9:20 | 7:55 | ~14.5 | ~6.5 | 3.65–≥9.0 | 7.0–8.0 |
| 8 Nov. 1987 | 1410 | 122 | 120 | 121 | 1 | | yes | yes | E | no? | | 2.5 (2.3) | 5:10 | 9:10 | 13 | 4 | 4.45–18.2 | 15.9 |
| 12 Feb. 1988 | 1234 | 137 | 132 | 124 | 13 | E | no | yes | E | yes | P | 2.2 (3.0) | 4:00 | 1:30 | ≥3:15 | ≥1:45 | | |
| 6 May 1988 | 0245 | 255 | 247 | 246 | 9 | P | yes? | ? | N | no? | | 1.5 (4.2) | 1:50 | 1:15 | ? | | | |
| 6 May 1988 | 1834 | 136 | 140 | 141 | 5 | P | yes | yes | E | yes | E | 3.0 (2.6) | 8:30 | 0 | 23 | 23 | 2.0–19.5 | 2.0–9.0 |
| 23 Aug. 1988 | 1841 | 78 | ? | 67 | 9 | P | yes | | | | | 3.4 (1.8) | 1:30 | 0:35 | ≥4 | ≥3:25 | | |
| 24 Aug. 1988 | 0057 | 100 | 101 | 98 | 2 | E | yes | yes | P | no | | 3.2 (2.2) | ? | 0 | ≥7:30 | ≥7:30 | | |
| 14 Sept. 1988 | 1812 | 82 | 77 | 58 | 24 | P | no | yes | E | yes? | E | 2.2 (1.8) | | 2:30 | 5:35 | 3 | | |
| 15 Sept. 1988 | 1117 | 107 | 114 | 112 | 5 | P | yes | yes? | E | no | | 2.7 (2.0) | 15:00 | 0 | >5 | >5 | 3.2–9.4 | 3.2–9.4 |
| 16 Nov. 1988 | 0948 | 307 | 301 | 295 | 12 | E | yes | no | | no | | 4.7 (2.0) | | | | | 1.7–>5.25 | 1.7–>5.25 |
| 21 Nov. 1988 | 0909 | 230 | 231 | 222 | 8 | P | yes? | yes | E | no | | 2.5 (1.8) | 7:15 | 5.25 | >21 | >15.5 | 4.6–>16.8 | 8.65–16.4 |
| 19 Dec. 1988 | 1702 | 237 | 230 | 232 | 5 | P | yes | no | | | | 5.1 (2.5) | 15:20 | 6:20 | ≥8:30 | ≥2:10 | 4.0–>7.6 | 4.0–6.7 |
| 24 Dec. 1988 | 1817 | 257 | 239 | 247 | 10 | P | yes | yes | E | no | | 1.3 (1.9) | 6:50 | 0 | 3 | 3 | 3.2–10.6 | 3.2–10.6 |
| 8 Jan. 1989 | 0501 | 60 | 45 | 47 | 13 | P | yes | yes | E | no | | 2.2 (1.8) | ~1:50 | 4:40 | 9 | 5:20 | | |
| 18 Feb. 1989 | 1957 | 147 | 135 | 138 | 9 | E | yes | yes | P | no | | 2.4 (1.8) | 4:30 | 10:30 | ? | | | |
| 2 June 1989 | 1124 | 323 | 327 | 333 | 10 | P | yes | ? | | no | | 1.4 (2.0) | 12:00 | ~8:00 | ~1.5d | ~2.8d | ??? | ??? |
| 6 Oct. 1989 | 1540 | 275 | 261 | 261 | 14 | P | yes | no | | yes? | P | 2.9 (2.0) | 13:45 | ? | 7 | | ??? | ??? |
| 7 Oct. 1989 | 0050 | 275 | 261 | 261 | 14 | P | yes | yes | P | no | | 2.5 (2.1) | 15:15 | 7:45 | ~15 | ~7 | ??? | ??? |

**Table 3.** Summary of Ray Measurements

| Unit | Mean or Percent | Range | Number | Comments |
|---|---|---|---|---|
| Width, deg | 2.5 | 1.3–5.1 | 27 | |
| Height of measurement, $R_L$ | 1.2 | 0.8–3.2 | 27 | measured at lowest height |
| Offset CME to ray axis, deg | 9.1 | 1–24 | 27 | 74% (20 of 27) poleward of CME |
| Ray alignment, % | 75 of rays | coaxial with CDE | 27 | |
| | 76 of rays | nonradial | 25 | 79% (15 of 19) toward equator |
| Ray motion | none in 13 | | 23 | |
| | six equatorward | four poleward | | motion-cycle-dependent? |
| Duration CME onset to CDE, hours | 7.9 | 1.5–15.3 | 22 | |
| Duration CDE to ray onset, hours | 3.8 | 0–10.5 | 24 | |
| Duration CDE to ray end, hours | >11.6 | 3–36 | 23 | |
| Ray lifetime, hours | >7.8 | | 23 | |
| Ray length at onset,[a] $R_S$ | 3.25 | 1.7–4.6 | 15 | |
| Ray length at end,[a] $R_S$ | >11.3 | >5.5–>21.4 | 14 | |

[a]See Figure 9.

detectable to the eye in a movie presentation as a separate feature contiguous with its observation on the images before or after. Columns 14–17 of Table 2 involve these time markers (all times are in UT). In column 14 is the time interval between the CME onset and the CDE end. Columns 15 and 16 list the time intervals between the CDE end and the ray onset and between the CDE end and the ray end. The difference between these two times is defined as the ray lifetime and given in column 17. Note that in four cases the time difference in column 15 was 0, indicating that in these events the ray was visible in the same frame as the CDE.

[34] Because of various uncertainties, these time differences are listed with a resolution of 5–10 min. We do not list any formal error or uncertainty with these times. After the repair of the SMM by the space shuttle crew in mid-1984, the HAO coronagraph maintained a high duty cycle for once-an-orbit observations of the complete corona [see *MacQueen and St. Cyr*, 1991]. Thus in general, a feature's "first-observed" time means it was not seen on the previous image which is usually no earlier than one orbit, or 95 min before. Likewise for a "last-observed" time. There were extended data gaps, usually leading to the greater than or less than symbols in the table. The ray end time was the most difficult to quantify since the ray typically faded gradually into the background. The overall ability to detect and measure features was discussed by *Burkepile and St. Cyr* [1993] and involves the feature's sharpness, the change in position of the occulting disk diffraction pattern between images, the use of images from different mirror sectors, the image quality which includes the severity of the electronic artifacts and horizontal streaking, and how well a feature can be followed from image to image. The overall quality of the set of images for a given event, especially of the CDE ray observations, is noted in Table 1.

[35] As shown in Table 3, the mean intervals between CME onset and the CDE, CDE end and ray onset, and CDE end and ray end were 7.9, 3.8, and $\geq$11.6 hours, respectively, with the ranges also noted. Histograms of the last two intervals plus that of the difference between them or the ray lifetime are shown in Figure 7. As discussed above, because of data gaps and the difficulty in determining the end time of some rays we could establish only lower limits for about a third of the CDE end to ray end intervals and the subsequent lifetimes.

[36] Finally, in columns 18 and 19 of Table 2 we give two values for the measured length of each ray. The first is the length measured over the lifetime of each ray and the second is the length during the time when the ray was well enough defined for us to make width measurements. The ray lengths were derived from height-time plots such as Figures 4 and 6. This was done under the important assumption that at any given time during its lifetime, the ray always extended from the solar surface, i.e., limb, to the base of the CDE. The base of the CDE is assumed to propagate outward at the speed dictated by the height-time curve fitted to and extrapolated outward from its observed points. In terms of the Lin and Forbes model (Figure 2 and below), we are measuring the distance $q$ from the surface to the base of the flux rope. Ideally we would like to know the length of the current sheet, $q - p$, but any associated surface arcade usually is not visible above the coronagraph's

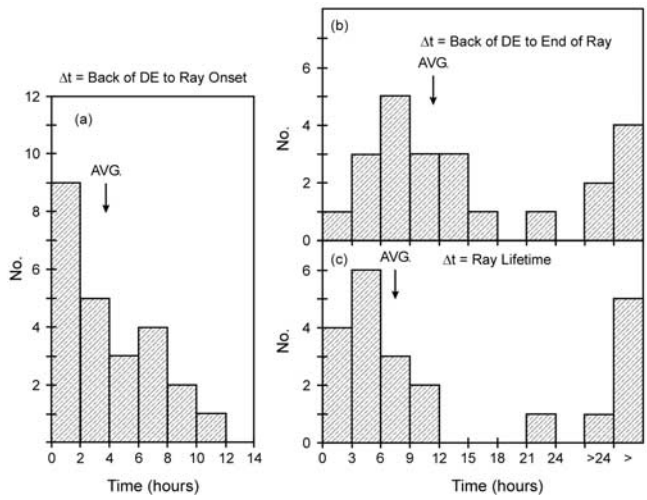


**Figure 7.** Histograms of the time intervals in hours between time markers for the transient rays: (a) between the end of the CDE and ray onset; (b) between the end of the CDE and the end of the ray; and (c) the difference between these two values, equivalent to the ray lifetime. The averages are marked by the arrows. In Figures 7b and 7c the last two columns give the number of rays having only lower limits for the CDE end to ray end intervals and the subsequent lifetimes. Events 7 and 25 had lifetimes >24 hours.

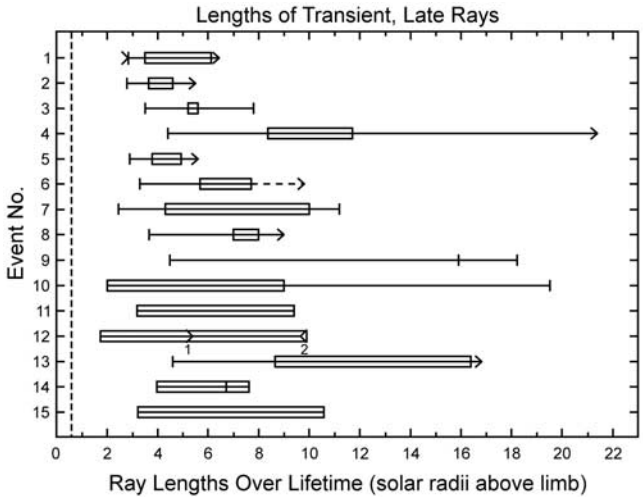


**Figure 8.** The estimated length of each ray from its onset time to its end time. The length in solar radii above the limb of each event ray is plotted keyed to the number of each event from Table 1. The solid horizontal lines show the length measured over the lifetime of each ray, and the shaded region denotes the length during the time range when the ray was well enough defined for us to make width measurements (i.e., the times with asterisks on the height-time plots). The onset and end times of the rays are marked by the short vertical lines, and the arrows mark lower or upper limits for the onset or end times.

occulting disk at 0.6 $R_L$. Thus in most cases $p$ cannot be directly measured, but must be $\leq 0.6\ R_L$.

[37] Table 3 shows that the mean (assumed) length of a ray ranged from 3.25 $R_S$ at ray onset to >11.3 $R_S$ at ray end, with the ranges given. Although the mean of the difference between the estimated ray lengths at their last visible time and at their onset time is about 8 $R_S$, the lengths in each event exhibited a very large range. This variation is illustrated in the bar graph of Figure 8. The (assumed) length in solar radii above the limb of each event ray is plotted keyed to the number of each event from Table 1. The solid horizontal lines show the length measured over the lifetime of each ray (Table 2, column 18) and the shaded region the length during the times when we made width measurements Table 2, column 19). Note that for many of the rays we could only determine a lower limit for the end (last observed) time.

### 3.3. MLSO Observations of the Low Corona

[38] Observations of the low corona from 1.2 to 2.2 $R_S$ with the HAO MLSO Mark-3 K-coronameter in Hawaii were occasionally available during the 1984–1989 period to complement the SMM coronagraph observations. Although these data could only be acquired for about 5 hours toward the end of each (UT) day and were generally of lower quality than the spaceborne SMM data, they were useful in studying the lower coronal evolution of the CMEs and CDEs. For the transient rays, the MLSO data were useful for confirming detection of the lower portions of the rays and whether or not a new streamer had formed at the base of the ray after the CME-CDE event. An advantage we had was that the rays appeared hours after the CME and were relatively long lived. As pointed out by *Kahler and Hundhausen* [1992], the appearance and growth of a new streamer, especially with a ray emanating outward from it, is indicative of reconnection in a current sheet and the subsequent closing of the loops below it to form an arcade. Thus such observations lend support to CME reconnection models requiring current sheets. In addition, measurements of the height of the top of the new streamer arcade give estimates of the parameter, $p$, in the Lin and Forbes model, which can then be used to calculate the current sheet length, $q - p$. Unfortunately, $p$ could be estimated for only those few of our events for which we had both adequate MLSO data and observations of a new streamer related to the CME-CDE.

[39] In Table 4 we summarize the MLSO and other ground-based observations of activity likely associated with the CME-CDE events. Before 1987 the MLSO MK3 data were not routinely archived unless an event had been noted by the observer on duty. However, at least one daily synoptic image was archived when observations were obtained. For our study we only examined the 18 ray events from Table 1 for which we had at least one synoptic MK3 image on the day of the CME and for 1 or more days following its onset. For these 18 events we repeat the event number from Table 1 in the first column of Table 4. In column 2 we list whether or not we think a new streamer appeared which was associated with the prior CME-CDE. An association was assumed if the new streamer was approximately coaligned with the axis of the CME and/or CDE, if it appeared within ~2 days of CME onset, and if it appeared to be growing with time. Column 3 indicates the six cases (Nos. 5, 11, 15–18, 20) in which we think the same transient ray observed by SMM was also visible in the MK3 field of view. Figure 5 shows one of these six events, number 18. The remaining columns provide data from the NOAA Solar-Geophysical Data Bulletins on pertinent observations of prominence activity and optical and X-ray flares that may have been associated with the CMEs. Columns 4–7 list the date and time, location and type of prominence activity, columns 8–10 list the time, location and intensity of Hα flares, and columns 11–12 list the peak intensity and duration of any associated GOES soft X-ray events.

[40] Summarizing the results of Table 4, in half (nine) of these events a new streamer likely or possibly developed after the CME-CDE, in 7 a new streamer was not observed, and the other two were uncertain. The six events in which the SMM ray was also detected in MK3 were evenly distributed as to whether or not they appeared to connect to a new streamer. Most of the SMM ray events had no obvious associated surface activity. This is perhaps not surprising since on the order of half the events might have surface activity that was poorly observed near the limb or was occulted by the limb. Five of the events (numbers 2, 3, 12, 15/16, and 24) were associated with erupting prominences either from ground based observatories and/or as a bright inner core within the SMM CME. Event five had an associated loop prominence system and a 1F/M1.0 long-duration X-ray flare. Four other events (numbers 13, 14, 17, and 18) were associated with active prominence regions, though not necessarily with eruptions. Therefore 1/3 of the

**Table 4.** Associated Surface and Low Coronal Activity

| | Mauna Loa Solar Observatory | | | Erupting Prominence | | | Hα Flare | | | X ray | |
|---|---|---|---|---|---|---|---|---|---|---|---|
| No. | New Strength? | Ray? | Date | Time, UT | Location | Type[a] | Time, UT | Location | Intensity[b] | Intensity | Duration, hours |
| 2 | no? | no | 18 Oct. | 0055–0414 | N14EL | APR[c] | none | | | none | |
| 3 | yes | no | 14 Nov. | 0415–0644 | S27EL | EPL | none | | | Sm | ≥1 |
| 5 | yes? | yes | 13–14 Feb. | | 00WL | LPS | 13,0250 | N04W63 | 1F | M1.0 | ~8 |
| 6 | yes | no | none | | | | none | | | no? | |
| 7 | yes | no | none | | | | no? | | | no? | |
| 8 | no? | no | none | | | | no | | | no? | |
| 11 | no | yes? | none | | | | (7,1500 | S24E48 | 1N) | C1 | sh. |
| 12 | no | no | 12 Feb. | <0530 | S60EL | EPL[c] | no | | (PCP[d]) | | |
| 13 | no | no | 6 May | 0010–>0800 | S55WL | APR | (2231 | S23W80 | 1F)PCP[d] | (B9 | ~1 |
| 14 | yes? | no | 7 May | 0104 to all day | S35EL | APR | no | | | no? | |
| 15–16 | ? | yes | 23 Aug. | <1630 | N15EL | EPL3 | 1800 | N24E88 | sF | M2.4 | 7 |
| 17 | ? | yes? | 14 Sept. | <1330>1655 | N18EL | APR | no | | | B7 | ~1 |
| 18 | no? | yes? | 15 Sept. | <2310 | S13EL | APR | no | | | none | |
| 19 | yes | no | none | | | | no? | | | none? | |
| 20 | yes | yes | none | | | | no | | PCP? [d] | (C1,2050 | sh) |
| 22 | no | no | none | | | | no? | | | (M1,1340 | ~1) |
| 24 | yes? | no | (18 Feb. | <0830 | S20EL | APR)[c] | no | | | no? | |
| 25 | yes? | no | none | | | | no | | | none | |

[a]APR, active prominence region; EPL, erupting prominence at limb; LPS, loop prominence system.
[b]Hα flare intensity is its brightness and area.
[c]Erupting prominence was seen in the SMM coronagraph field of view.
[d]Polar crown prominence.

SMM ray events with MLSO data (6 of 18) could be associated with eruptive activity, another four with possible activity, and the remaining eight with no evident activity. Two of the rays also observed in MK3 (numbers 5 and 15/16) were associated with eruptive activity, two with possible activity, and two with no activity.

## 4. Comparisons With Model Predictions

### 4.1. Overview of Models

[41] Most models of CMEs are based on the principle that they are caused by a sudden release of magnetic energy stored in the corona. The continual emergence of new flux from the convection zone and the shuffling of the footpoints of closed field lines cause stresses to build up in the coronal field. Eventually, these stresses exceed a threshold beyond which a stable equilibrium cannot be maintained, and the field erupts. The eruption releases magnetic energy stored in fields created by coronal currents, so models based on this mechanism are sometimes referred to as "storage" models.

[42] When comparing observations with the various CME models, it is important to keep in mind that all the models that have been developed so far focus on specific aspects of the CME phenomena. Some are primarily designed to account for the observed structure of the CME [e.g., *Gibson and Low*, 1998], while others [e.g., *Wu et al.*, 1995] apply only to the post eruptive dynamics and do not incorporate a realistic trigger mechanism. Storage models that do address the issue of CME onset differ from one another in the way that they account for the loss of equilibrium, or stability, of the coronal magnetic field. Some models [e.g., *Sturrock et al.*, 2001] assume that the mechanism that initially triggers the magnetic energy release is purely an ideal one, that is, one which does not require a violation of the frozen-flux condition. Other models [e.g., *Antiochos et al.*, 1999] use a nonideal MHD process, usually magnetic reconnection, to trigger the eruption. However, even models which use a purely ideal MHD process to initiate an eruption must incorporate nonideal MHD processes at some point in time to account for plasma heating and particle acceleration [*Priest and Forbes*, 2000].

[43] Since in this paper we are considering the formation and evolution of current sheets that might be produced by CMEs, we need to consider models which explicitly include such sheets. For this purpose we use two closely related models. The first is the analytical model of *Lin and Forbes* [2000] and the second is the numerical model of *Linker et al.* [2003]. Both models are based on force-free arcades, which contain a flux rope that loses equilibrium in response to changes in the photospheric magnetic field. The loss of equilibrium, quickly leads to the formation of a current sheet which undergoes reconnection.

### 4.2. Lin and Forbes Model

[44] This two-dimensional model consists of a force-free flux rope suspended in the corona by a balance between magnetic compression and tension forces. The photosphere (or, more properly, the base of the corona) is located at $y = 0$ in the $x$-$y$ plane. An eruption is triggered by slowly changing the normal magnetic field, $By(x, 0, t)$, at the photosphere so that a balance between compression and tension is no longer possible. Many possibilities exist for the functional form of $By(x, 0, t)$, but most lead to equations that can only be solved numerically. However, there are a few special cases that lead to closed-form analytical solutions [see *Forbes et al.*, 1994]. One of the simplest is

$$B_y(x, 0, t) = A_0\{\delta[x - \lambda(t)] - \delta[x + \lambda(t)]\}, \quad (1)$$

which corresponds to positive and negative line sources located at $x = \pm\lambda$. These sources produce a simple arcade with a net flux of $-A_0$ across the $y$ axis, and this flux remains invariant during the evolution of the configuration.

This particular form of $By(x, 0, t)$ does not require any reconnection associated with emergence, or submergence, of the photospheric field to trigger an eruption. However, some of the alternate forms of $By(x, 0, t)$ considered by other authors [e.g., *Forbes and Isenberg*, 1991; *Lin et al.*, 1998; see also *Linker et al.*, 2001] do incorporate such reconnection. Eruption in the Lin and Forbes model is triggered by decreasing the distance, $2\lambda$, below a critical value.

[45] Within the arcade produced by the two line sources there is a force-free flux rope with radius $r$ located at a height $h$ on the y axis. Only after onset of the eruption does a current sheet form in this model. The lower tip of the current sheet is located at $y = p$ and the upper tip at $y = q$ (see Figure 2). The mathematical form of the model field in the region exterior to the flux rope is

$$B_y + iB_x = \frac{2iA_0\lambda\left(h^2+\lambda^2\right)\sqrt{(z^2+p^2)(z^2+q^2)}}{\pi\left(z^2-\lambda^2\right)(z^2+h^2)\sqrt{\left(\lambda^2+p^2\right)\left(\lambda^2+q^2\right)}}, \quad (2)$$

where $z = x + iy$, $y > 0$, and $|z - ih| > r$. Inside the flux rope the field is prescribed by a flux rope solution due to *Parker* [1974]. The most significant aspect of this solution is that it gives the relation between the flux rope current, $I$, and its radius, $r$. For small values of $r$ (i.e., $r \ll \lambda$), this relation is

$$r \approx r_0(cA_0)/(\pi I), \quad (3)$$

where $r_0$ is a free parameter giving the radius of the flux rope when $I = cA_0/\pi$. In terms of $h$, $p$, and $q$, the current $I$ is

$$I = \frac{c\lambda A_0}{2\pi h}\frac{\sqrt{(h^2-p^2)(h^2-q^2)}}{\sqrt{(\lambda^2+p^2)(\lambda^2+q^2)}}. \quad (4)$$

[46] The evolution of the model configuration is obtained by application of Newton's second law and Faraday's equation for magnetic induction. These are used to determine the three unknowns, $p$, $q$, and $h$ as functions of time. The flux rope is treated as a simple projectile driven by the magnetic Lorentz force, $(\mathbf{J} \times \mathbf{B}/c)$, and so the model does not include the wave dynamics associated with a plasma. Line-tied boundary conditions are applied, so that there is no injection of flux or magnetic energy once the eruption starts. (See *Lin and Forbes* [2000] for further details.)

[47] The reconnection rate at the current sheet is prescribed by $M_A$, the inflow Alfven Mach number at the midpoint of the current sheet. Although, *Lin and Forbes* [2000] assume that $M_A$ is a constant, one can, in principle, allow $M_A$ to be a function of time. Determination of this function self-consistently requires a time-dependent theory of strongly driven reconnection, but such a theory does not exist at the present time. However, it is known that for a low-$\beta$ plasma, like the corona, $M_A$ must lie somewhere in the range between zero and unity. Observations [*Poletto and Kopp*, 1986; *Ciaravella et al.*, 2002] indicate that $M_A$ is on the order of $10^{-1}$ during the acceleration phase of the CME, but that later on $M_A$ drops to values below $10^{-3}$ [see also *Lin et al.*, 1995; *Yokoyama et al.*, 2001].

[48] In the Lin and Forbes model the flux rope cannot escape the Sun unless $M_A$ is sufficiently large. Without some reconnection, the magnetic tension in the field lines will eventually halt the outward progress of the rope. For very fast CMEs (speeds >1000 km s$^{-1}$), $M_A$ must be greater than about 0.05, but for slower CMEs much smaller values suffice since the rate at which the current sheet grows is correspondingly smaller.

[49] The Lin and Forbes model depends on several other parameters. These are $\lambda$, the half-distance between the sources at onset; $m$, the CME mass/unit length; $A_0$, the flux per unit length produced by one of the photospheric line sources; and $r_0$, the initial radius of the flux rope. In addition to these, a small perturbation, either in the form of a velocity, or a displacement, needs to be specified in order to initiate the movement of the flux rope away from the unstable equilibrium at the critical point.

[50] A key aspect of the Lin and Forbes model is the value of the Alfven speed at the midpoint location of the current sheet, since the speed is important in determining how fast the opened field lines reconnect. To determine this speed it is necessary to incorporate a coronal density model. *Lin and Forbes* [2000] considered two different density models, one with uniform density and the other with a density which decreased exponentially with altitude. However, since neither f these models is suitable for altitudes more than a solar radius above the surface, in this paper we have used the empirical density model of *Sittler and Guhathakurta* [1999]. This model gives a density which decreases exponentially close to the Sun but which changes over to the inverse square of the distance beyond one solar radius [see also *Lin*, 2002]. This more realistic density model leads to an Alfven speed at four solar radii which is more than four orders of magnitude lower than the Alfven speed in the exponential model. As a consequence, the rapid disappearance of the current sheet seen in some of the *Lin and Forbes* [2000] cases a few hours after onset, no longer occurs.

[51] Figure 9 shows an example of the evolution predicted by the *Lin and Forbes* [2000] model using the *Sittler and Guhathakurta* [1999] density model. Here the parameters have been chosen to give a terminal CME velocity, $V_T$, of 300 km s$^{-1}$, similar to cases numbers 11 and 12 in Table 1 (but greater than the average of all the events). In the model the terminal velocity corresponds to the conversion of all the free magnetic energy in the system into kinetic energy, and it is a theoretical upper limit on the speed of the flux rope. The formula for $V_T$ is

$$V_T = \frac{A_0}{\pi m^{1/2}}\left[\frac{3}{2} + 2\ln(2\lambda/r_0)\right]^{1/2}, \quad (5)$$

which gives $V_T \approx 300$ km s$^{-1}$ when $\lambda = 5 \times 10^4$ km, $m = 2 \times 10^6$ gm/cm, $A_0/\lambda = 10$ G, and $r_0 = 0.1\ \lambda$. The time between the loss of equilibrium and the appearance of the $x$ line is primarily determined by the size of the initial velocity perturbation, $v_0$ (here it is 100 m s$^{-1}$).

[52] The rate at which the lower tip of the current sheet at $p$ rises is controlled primarily by the rate of reconnection (here $M_A = 0.1$), and so it rises very slowly. By contrast, the upper tip of the current sheet at $q$ rises at a rate that is only about a factor of two smaller than the speed at which the flux rope moves. Consequently, a very long current sheet

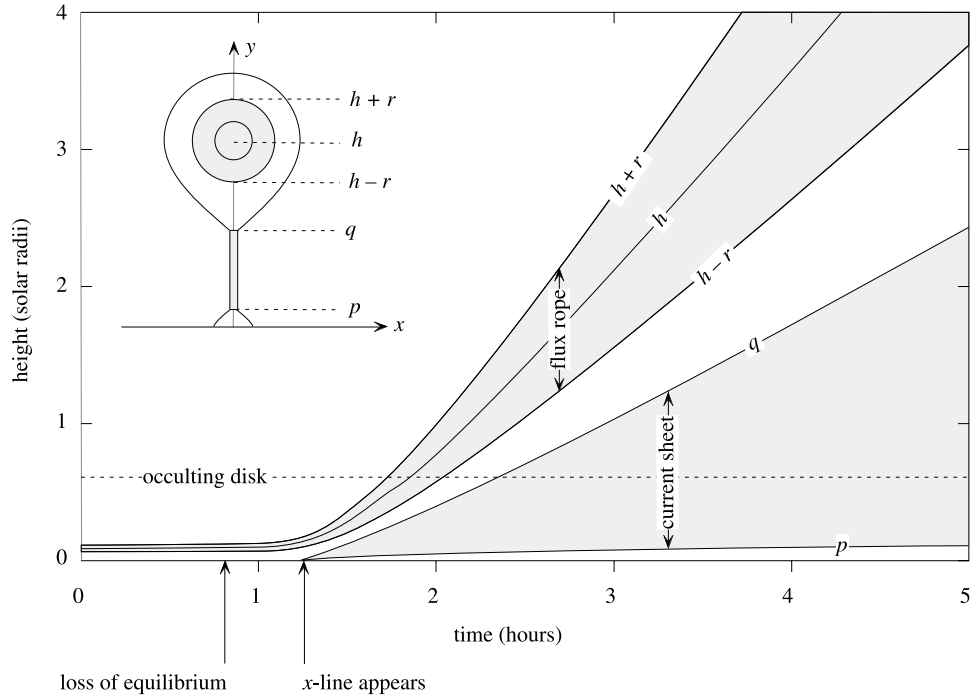


**Figure 9.** Current sheet evolution predicted by the *Lin and Forbes* [2000] model for $\lambda = 5 \times 10^4$ km, $m = 2 \times 10^6$ gm/cm, $A_0 = 10$ G, $r_0 = 0.1\ \lambda$, and $M_A = 0.1$. An initial perturbation velocity of 100 m s$^{-1}$ is used to disturb the unstable equilibrium at the critical point.

forms. In order for a long sheet not to form, $M_A$ would have to have a value in excess of 10, but such a value is physically implausible because it would require the plasma to flow into the current sheet at hyper Alfvenic speeds in contradiction with both theory [e.g., *Parker*, 1957] and observations [e.g., *Yokoyama et al.*, 2001]. Thus one of the firm predictions of the *Lin and Forbes* [2000] model is that a long current sheet should form.

[53] The lifetime and extent of the current sheet in the Lin and Forbes model is consistent with our interpretation here of the rays as current sheets. The observed lifetimes of the rays are on the order of 8 hours (see Table 3), and the rays in all cases extend out beyond the field of view of the SMM coronagraph before they disappear. Using the speed of the CDE to extrapolate the position of the ray out beyond the field of view implies ray lengths in excess of 11 solar radii. These average values are in a good agreement with Lin and Forbes. There are a few rays, such as the one observed on 24 May 1987 at 1505 UT, which have a lifetime that appears to be too short to be consistent with the model, but these cases may be due to the fact that these rays have evolved to a state in which they are no longer detectable by the SMM coronagraph. The Lin and Forbes model only predicts the locations of the tips of the current sheet as a function of time, and it does not provide any prediction about how hot or dense the current sheet should be, nor does it provide any prediction about the extent of the current sheet in the direction out of the plane of the observations. To make such predictions a more realistic model is needed.

### 4.3. Linker et al. Model

[54] *Linker et al.* [2003] have developed a numerical model, which is based on the same principles as the analytic *Lin and Forbes* [2000] model, but that provides a much more realistic treatment of the dynamics of the eruption. Unlike the analytical model, the numerical model incorporates MHD waves including the formation of a fast-mode shock wave in front of the CME. The numerical model also includes gravity, a stratified atmosphere, a spherical geometry, an overlying helmet streamer, and a polytropic solar wind model with $\gamma$, the polytropic index, set to 1.05. In the example discussed here the configuration has axial symmetry, but nonsymmetric simulations have also been carried out which show similar behavior [*Amari et al.*, 2000; *Roussev et al.*, 2002]. Reconnection in these simulations is determined by numerical resistivity, which can vary in both space and time in ways that are not related to any physical processes. However, except for this aspect, the reconnection dynamics is self-consistently determined.

[55] Figure 10 shows simulation results for a case corresponding to a CME that had accelerated to $\sim$400 km s$^{-1}$ by 3 $R_S$. The radial magnetic field at the surface is on the order of ±0.25 Gauss near the poles, reaching a maximum of ±3.8 Gauss near the equator. The inferred rate of reconnection in the numerical simulation corresponds to an inflow Alfven Mach number at the current sheet on the order of 0.1. Details of this simulation, including its extension into the inner heliosphere, have been presented elsewhere [*Riley et al.*, 2002; *Odstrcil et al.*, 2002; *Riley et al.*, 2003].

[56] As the field at the surface reconnects it entrains cool, dense material so that, at onset, the flux rope which has formed contains a prominence-like structure that is ejected along with the magnetic field and coronal plasma. Although the actual formation of a prominence in the corona likely

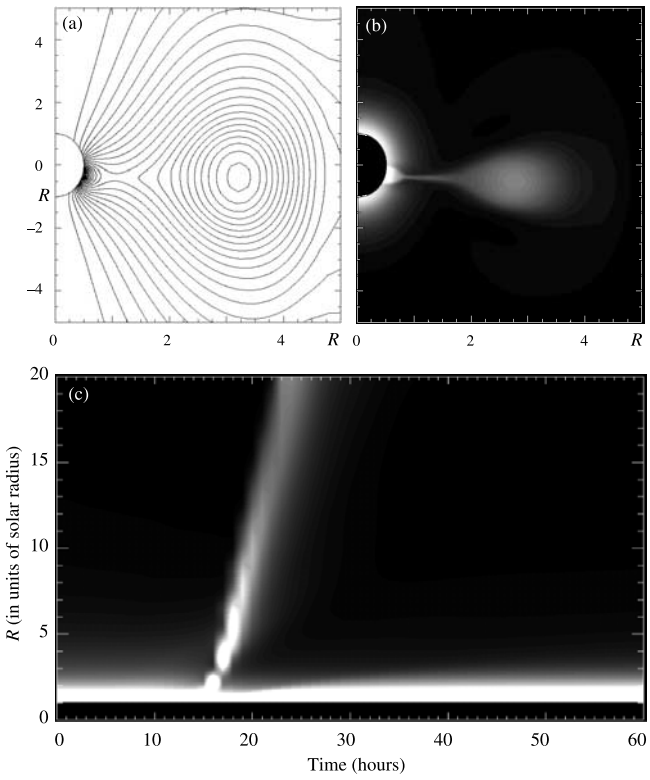


**Figure 10.** Results from a simulation run of the Linker et al. model for a CME with a speed of ~400 km $s^{-1}$. (a) The magnetic flux function (a fiduciary of magnetic field lines in two dimensions) at 17 hours following the end of the shearing phase. (b) Simulated polarized brightness image also at the same time. (c) Simulated time-height composite image of the polarized brightness, obtained by vertically stacking radial slices at approximately $-10°$ latitude sequentially in time.

involves a more complex interaction between thermal and dynamical process, the plasma configuration at the point of eruption in this numerical simulation is probably close to what one might expect for an erupting prominence.

[57] Figure 11 shows the lower and upper tips of the current sheet inferred from contours of the computed polarization brightness in the simulation model (e.g., Figure 10b). The locations of the tips inferred in this way differ somewhat from their actual positions because the outflow from the reconnection jet prevents the density from being distributed uniformly along the flux surfaces. Moreover, the locations of the current sheet tips inferred from observations are likely to show similar differences. These differences are sufficiently small that they do not effect our conclusion that the simulation confirms the presence of a long, sufficiently dense current sheet created in the aftermath of the CME. Just as in the Lin and Forbes model, the lower tip of the current sheet ($p$) rises very slowly with time, while the upper tip ($q$) rises rapidly with time at a speed that is no more than a factor of two slower than the CME itself, again in general agreement with the SMM observations.

[58] It is perhaps surprising that the analytically computed trajectories shown in Figure 9 are so similar to the numerically computed trajectories shown in Figures 10 and 11, given the simplicity of the model. By "similar" we mean that the trajectories of the flux rope and the upper and lower tips of the current sheet look qualitatively alike in the two models. The analytical model is for a straight flux rope suspended above an infinite, flat plane. It excludes several physical effects that occur in the numerical simulation, such as gravity and the interaction of the flux rope with the solar wind. So why should the trajectories look so similar in their form?

[59] In hindsight, the close similarity can be understood from the fact that both models are storage models which means that the main magnetic force acting on the flux rope occurs within a few solar radii of the Sun. Acceleration beyond this distance is due to secondary forces, such as the pull of the current sheet, gravity, and solar wind interaction. As long as the reconnection rate is sufficiently fast ($M_A > 0.01$), the deceleration caused by the current sheet is negligible. Since gravity falls off as $h^{-2}$, whereas the magnetic forces fall off, $\ln(h/r)$, as $h^{-1}$ in the numerical model [*Shafranov*, 1966] and $h^{-1}$ in the analytical model [*Forbes and Isenberg*, 1991], gravity is relatively negligible beyond about a solar radius. Only the interaction with the solar wind is likely to be important at large distances, but for the case shown in Figures 10 and 11, the flux rope speed is nearly the same as the solar wind speed, so little interaction occurs. However, other numerical simulations involving flux ropes that move much slower or faster than the solar wind do show the expected acceleration or deceleration that results from this interaction [e.g., *Cargill and Schmidt*, 2002].

[60] One aspect of the observations which neither the Lin and Forbes nor the Linker et al. model accounts for is the sudden brightening of a ray several hours after its apparent formation (~4 hours, see Table 3). The brightening itself is not well understood. It could be due either to an increase in the density of the current sheet, or to an increase in the thickness of the sheet along the line of sight. Since neither model incorporates a physically realistic model of the reconnection process occurring in the current sheet, it may be that this brightening has something to do with a change in the reconnection rate after several hours. For example, if

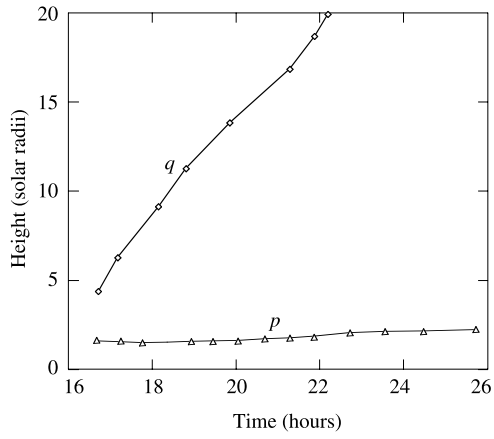


**Figure 11.** Time versus height profiles of the tip of the reforming streamer ($p$) and the location ($q$) where the antisunward edge of the reconnection site meets the concave-outward field lines of the flux rope.

the rate of reconnection were suddenly to decrease, then according to the Sweet-Parker theory [*Parker*, 1957], the sheet thickness should increase. This increase would lead to an increase in the apparent brightness when the sheet is viewed at an angle other than end-on.

## 5. Conclusions

### 5.1. Summary

[61] The main conclusions of this study are as follows. Several prior studies of white light coronagraph observations of coronal structures in the wake of CMEs, notably *Webb and Cliver* [1995], found evidence of the possible disconnection of magnetic field lines in ~10% of all CMEs. This rate includes our previously unpublished survey of CMEs observed by the SMM coronagraph from 1984–1989 and presented in Appendix A. The candidate disconnection events (CDEs) consist of concave-outward structures, either as arcs or as the base of a complete circular structure. The more sensitive LASCO CME observations suggest that the rate of detection of such features may be as high as 50% during nonmaximum phases of the solar cycle.

[62] In a survey of the SMM CME CDEs, we found that in about half (26) of the events coaxial, bright, narrow transient rays formed relatively suddenly in the wake of the CME and CDE, then faded or disappeared hours later. In light of previous observational studies and CME models invoking reconnection, our working hypothesis is that these rays are associated with extended and long-lived current sheets forming as a result of reconnection behind the main CME. To our knowledge, this is the first time that a survey of ray-like structures has been performed and the results compared with CME reconnection models.

[63] We studied the relationship of the SMM CDEs, with or without later rays, to their associated CME and to any preexisting structures, primarily coronal streamers. On average the CDEs, with or without rays, were about a factor of two narrower and slower than their accompanying CMEs. The spans of these CMEs were slightly lower than those of typical SMM CMEs. However, the mean speed of the CMEs having CDEs and rays was significantly slower (218 km $s^{-1}$) than the mean of the leading edges of all SMM CMEs (350 km $s^{-1}$ [*Hundhausen et al.*, 1994]). In terms of preexisting structures, 81% of the CMEs having CDEs with rays significantly disrupted an associated streamer, and in half of the cases the streamer was completely blown out or destroyed. This disruption rate was greater than that of the full sample of SMM CDEs (see Appendix A).

[64] We analyzed the CDE and associated ray structures in terms of their heights and lengths, widths, alignments and motions, and brightness variations all as functions of time. The mean width of the rays was 2.5° when measured at the lowest height above the occulter, an average of 1.2 $R_S$ above the limb. For a given ray, there was some variation of its width with height and time but not in a systematic way. The rays were offset from the axes of their associated CMEs by an average of ~9° in the poleward direction. Although coaxial with their associated CDEs, the rays tended to extend outward nonradially and be tilted equatorward. Some of the rays exhibited lateral motion and this motion seemed somewhat solar-cycle-dependent.

[65] We used height and time data related to the CDEs and the appearance and disappearance of the rays to estimate the lengths and lifetimes of the rays (see section 3.2). On average the CDE followed the onset of the CME by ~8 hours and the transient ray appeared ~4 hours after the CDE was no longer visible, or ~12 hours after CME onset. The mean lifetime of a ray was ≥8 hours. However, these time durations varied considerably from event to event. The entire process from CME initiation to the fading of the "current sheet" appears to extend over a period of ~12 hours to 1.5 days. Assuming that at all times the observed ray extends to the base of the CDE, we estimate their mean length when first observed to be 3.25 $R_S$ above the limb, and when last detected to be >11 $R_S$, but again with a large event-to-event variation. This equates to the distance $q$ in the Lin and Forbes model. The length of the current sheet is determined by $q - p$, where $p$ is the top of any near-surface arcade, or newly forming streamer connecting to the ray. During the lifetime of a ray, no new streamer appeared above the occulting disk at 0.6 $R_S$ above the limb. However, in several events with MLSO MK3 data (e.g., Figure 5) the tip of a streamer extended outward to the edge of its field of view at ~1.2 $R_S$. Thus while the ray is visible, $p$ seems to be on the order of 1 $R_S$ or less in these events.

[66] Although we had only limited MLSO and other data to use to search for any near-surface activity that might have been associated with the CMEs having CDEs and rays, we could conclude the following. Half of the events with rays appeared to have newly forming streamers at the base of the rays. In about 1/3 or six of these cases, the SMM ray could also be observed near the surface in at least one MK3 image. About half of the ray events were also associated with surface activity, mostly in the form of eruptive or active prominences.

[67] In the last section we compared our measurements of the lengths and lifetimes of the transient rays with two closely related CME models which explicitly incorporate flux ropes and current sheets; the analytical model of *Lin and Forbes* [2000] and the numerical model of *Linker et al.* [2003]. These models require specification of a number of parameters. Nevertheless, we find that the models are consistent with the observations in the sense that they predict current sheets lasting for many hours and extending more than 5 $R_S$ into the outer corona. In this view the concave-outward structure which we call a CDE is the bottom coil(s) of a flux rope, below which is the Y reconnection surface at the top of the current sheet (see Figure 2). A similar inverse Y point connects the base of the sheet with the reforming surface arcade. Since neither model incorporates a physically realistic model of the reconnection process occurring in the current sheet, we cannot directly infer the width, density or temperature of the current sheet nor its lateral extent out of the plane of the sky of the observations. One aspect of the observations which is not expected from the models is the typical sudden brightening of a ray several hours after its apparent formation during eruption of the flux rope.

### 5.2. Discussion

[68] We find the average width of the rays to be 2.5° with a range of 1.3°–5.1°. This yields a distance in the plane of

the sky at about 1 $R_S$ above the limb of $6 \times 10^4$ km. This value is similar to the width of $10^5$ km of the "high-temperature region" (FeXVIII) measured in the two SOHO UVCS events discussed by *Ciaravella et al.* [2002] and *Ko et al.* [2003]. These regions were interpreted as being within current sheets between post-CME arcades near the surface and outward-moving flux rope/CMEs. The estimated width is likely an upper limit to the true width (J. Raymond, personal communication, 2003).

[69] The Lin and Forbes model does not specifically incorporate a model of the reconnection process occurring in the current sheet, but *Forbes and Lin* [2000] have used Sweet-Parker theory to estimate the current sheet thickness. Since the Sweet-Parker theory assumes a steady state, such an estimate is only valid when the speed at which the current sheet grows is small compared to the Alfven wave speed in the surrounding corona. According to the models we have discussed here, the growth speed of the sheet is essentially the same as the speed of the CDE structure and, as indicated in Table 1 and Figure A3, these range from 35 to 420 km $s^{-1}$ for our events. Recently, *Mann et al.* [2003] have estimated that the Alfven speed in the corona in the region from 1 to 5 $R_S$ above the solar surface is in the range 400–650 km $s^{-1}$, so estimates of the current sheet thickness using Sweet-Parker theory are likely to be meaningful only for our slower events with a CDE speed <200 km $s^{-1}$. Even for these cases it only provides a rough estimate since fractional errors on the order of the CDE speed divided by the Alfven speed will exist.

[70] According to Sweet-Parker theory, the current sheet thickness, $l$, is

$$l = (q - p)M_A. \tag{6}$$

[71] Analyses of the motion of flare ribbons and loops [*Poletto and Kopp*, 1986] and of reconnection-like flows observed by EIT below a CME [*Yokoyama et al.*, 2001] imply that $M_A$ has a peak value on the order of 0.03 which declines tens of minutes after onset to a value on the order of 0.001. Using the higher value of 0.03 and assuming a sheet length ($q - p$) of 5 $R_S$ ($3.5 \times 10^6$ km) yields a current sheet thickness, $l$, on the order of $10^5$ km. This is in good agreement with our white light measurements and with the UVCS FeXVII widths. Later in the event, as the flux rope continues to move out and the current sheet continues to lengthen, $M_A$ continues to decrease so the thickness of the current sheet will not necessarily increase. This is consistent with our result that a given ray shows no systematic change with either time or height. Eventually the ray should broaden as the magnetic field decreases and solar wind pressure begins to dominate. It will be of interest to measure similar bright rays in LASCO data since they can be followed much farther into the outer corona and over longer time periods.

[72] These predicted and measured sheet thicknesses are of the same order as the thickness of the tops of helmet streamers when viewed at their thinnest near solar minimum [*Wang et al.*, 1998b]. This is perhaps not surprising since a steady state neutral sheet must extend above coronal helmet streamers; in fact, the confluence of many such steamers in longitude around the Sun forms the base of the heliospheric current sheet which appears as a sector boundary crossing in space [e.g., *Crooker*, 2000]. *Wang et al.* [1998b] note that *Borrini et al.* [1981] found that the mean proton densities at sector boundaries at 1 AU have a narrow peak whose width is consistent with the $\leq 3°$ thickness of the streamer sheets near the Sun.

[73] Reconnection models like Lin and Forbes and Linker et al. imply that there should be a measurable inflow of plasma into the sides of a current sheet. From flux conservation arguments [*Forbes and Lin*, 2000], one can show that these flows should be roughly equal to the speed of the flare ribbons times the ratio of the magnetic field at the outer edge of the ribbons to the magnetic field in the corona in the vicinity of the $x$ line (within the sheet). Thus shortly after onset, when ribbon speeds as high as 50 km $s^{-1}$ are observed [*Moore et al.*, 1980], inflows of the same order could occur very low down for a few minutes. However, by the time the current sheet is visible in a coronagraph, ribbon speeds have slowed to values typically in the range 1–5 km $s^{-1}$, so inflows should be of this order, or possibly slightly larger depending on how the coronal field varies with height. Although inflows have not been typically observed [*Hudson and Khan*, 1996], there are recent observations of possibly related flows. For a CME on 18 March 1999, Yokoyama et al. [2001] derived an inflow speed toward the presumed $X$ point in the low corona of 5 km $s^{-1}$. *McKenzie* [2000] reported observations of dark X-ray downflows of a few hundred km $s^{-1}$ above limb flare arcades following CMEs. These could be related to the reconnection process, though probably not to the higher sheet inflows. We examined *Yokoyama et al.*'s [2001] event higher up and later in the LASCO C2 and C3 fields of view and could find no evidence of inward motions near the presumed current sheet. We also could not see any inward motions during the SMM ray events on movies of the events. That inflow was seen early in the Yokoyama event near the surface and is not detected later farther out in the corona is perhaps not surprising, since the slow ribbon speeds (<2 km $s^{-1}$) which exist a few hours after onset imply similarly slow inflows and the coronal density decreases with height. Thus the absence of observed inflows higher in the corona and later in the event is not unexpected in terms of the current sheet models.

[74] Other LASCO events reported as flux ropes or disconnection events have been discussed in the literature. *Simnett et al.* [1997], *Chen et al.* [1997], *Plunkett et al.* [2000], and *Ko et al.* [2003] have described events with characteristics similar to the SMM CDE-ray events. The CMEs all had circular structures with V or blob-shaped features at their base connected by a bright ray to the Sun. (Note that in these LASCO events, the rays extended through the C2 and C3 fields of view ($\leq 30$ $R_S$) to the backs of the CDEs, thus supporting our key assumption about measuring the SMM ray lengths.) Most of the LASCO events were streamer blowouts with a new streamer forming about 14 hours to 1 day later. The two events discussed by *Simnett et al.* [1997] and the single event by *Chen et al.* [1997] had speeds ranging from 50 to ~300 km $s^{-1}$ out to heights $\geq 25$ $R_S$. The CDEs exhibited significant acceleration starting at a height of 5–6 $R_S$ for the Simnett events and gradually over the entire range for the Chen and Plunkett events. The 2 June 1998 event discussed by *Plunkett et al.* [2000] involved a spectacular, fast erupting prominence in which the central ray appeared

about 12 hours after onset. The *Ko et al.* [2003] event was very fast and energetic with a spectacular streamer blowout followed by an extended ray which moved northward, lasting until another CME 1.5 days later. Thus considering both the SMM and LASCO results, it appears that, typically, CMEs with CDEs having extended, trailing rays may be part of a class of relatively slow CMEs which exhibit significant acceleration especially over the extended field of the LASCO C3 instrument. However, fast events with CDEs and rays also occur. Most events of this class involve preexisting streamers that are significantly disrupted or destroyed by the CME and have new streamers form and grow outward from near the surface starting about 12 hours after onset.

[75] We emphasize that CDEs, including features interpreted as flux ropes within CMEs, are also observed without any obvious coaxial, transient ray. As mentioned earlier, less than half of the SMM CMEs with CDEs had trailing rays. Studies of LASCO flux-rope-like CMEs that appear to have no central, bright, transient ray (and also no reforming streamer above the C2 occulter) include *Wood et al.* [1999], *Dere et al.* [1999], and *Ciaravella et al.* [2002]. And a bright, transient ray trailing the main CME can occur without the detection of an obvious CDE structure. See, for example, the SMM events in the work of *Kahler and Hundhausen* [1992, Figure 3, Figure 5] paper. Obviously observational factors can play a significant role in whether or not certain features of an eruption can be detected in a given waveband. In white light, the amount of dense plasma along the line of sight, the presence of background material, and the distance of the material from the plane of the sky all contribute to the detectability of coronal structures. If CDEs are interpreted as erupting flux ropes with current sheets beneath them, then the detection of the current sheet as a bright ray will depend on the density in the sheet as functions of time and height as well as the orientation of the plane of the sheet with regard to the viewing angle [e.g., *Forbes and Acton*, 1996]. In this context, it is interesting that in the 23 March 1998 event discussed by *Ciaravella et al.* [2002], the current sheet was apparently detected in the UVCS slit as a narrow, dense, hot feature despite the lack of detection of a corresponding ray-like structure in white light by LASCO.

[76] As we noted in section 2, *Kahler and Hundhausen* [1992] found that multiple ray-like structures were common following CME fronts, and some of the events we studied had several late rays. This raises the question whether or not these extended rays are related to the hot ''fans'' or spikes sometimes observed just above postflare loop arcades in Yohkoh and TRACE [e.g., *McKenzie and Hudson*, 1999; *McKenzie*, 2000]. Those authors speculate that the latter could be associated with strong, structured surface fields, but it is also possible that the spikes map into the extended rays. If so, they might represent denser, hotter plasma within a current sheet viewed more side-on; such a study is better addressed with the recent SOHO-era data.

[77] Areas of transient dimming of preexisting coronal emission against the solar disk are often observed in the Yohkoh and EIT data in association with eruptive arcades and CMEs [e.g., *Hudson and Webb*, 1997]. The dimmings are strongly associated with frontside halo CMEs [e.g, *Hudson et al.*, 1998], and probably are signatures of the depletion of mass above or adjacent to the long-lived arcades [e.g., *Harrison and Lyons*, 2000]. Such features were first observed on Skylab X-ray images and dubbed ''transient coronal holes'' by *Rust* [1983]. Although the dimming areas observed in soft X rays are usually small compared with the size of the subsequent CME, EIT difference images in 195 often reveal extended areas of weaker dimming which map out the surface footprint of an associated CME [*Thompson et al.*, 2000]. One interpretation is that the initially closed coronal field lines open during the initial phase of a CME, leaving the dimming in regions away from the bright arcade that marks the earliest reconnecting fields underneath the CME. The dimming area thus delineates the area of magnetic field lines temporally opened during the CME which gradually disappears, or returns to its preexisting level of coronal emission, as the fields outside of the central arcade close down. Attempts to find evidence of these open fields behind the CME in interplanetary space have not been very successful, except that *Neugebauer et al.* [1997] found quiet radial fields and/or periods of outward-propagating Alfven waves, both expected from large-scale coronal holes, trailing many ISEE-3 interplanetary CMEs. The estimated lifetimes of transient coronal dimmings range from $\sim$5 hours to $<$2 days (Skylab [*Rust*, 1983]; Yohkoh (*Kahler and Hudson* [2001] and one of us, D. F. Webb)). In the context of this paper, these times are consistent with the range of lifetimes found for the transient rays. Thus we can speculate that the development and lifetime of the current sheet trailing a CME is related to the development and lifetime of the surface dimming region because both result from the partial reconnection of the rising CME/flux rope. Unfortunately, the transient rays are best viewed in limb events and we had no data on coronal dimmings available for the SMM events.

[78] *St. Cyr et al.* [2000] found that at least 36% (possibly as high as 48%) of LASCO CMEs exhibit a concave-outward feature later in the event. Since the LASCO coronagraphs are more sensitive than earlier ones, and considering that subtle CDE features may only be detectable for CMEs near the limb, this suggests the possibility that most CMEs contain such structures. This, in turn, suggests that reconnection/disconnection may be fundamental to the development of CMEs, although it also possible that such flux-rope-like structures form below the occulting disk,$<2$ $R_S$; that is, they either preexist near the surface or form very early in the eruption. A study of SOHO-era data should improve our understanding of reconnection and current sheets trailing CMEs because of the increased sensitivity and field of view of the LASCO coronagraphs and telescopes that view the surface and low corona features associated with the transient rays.

## Appendix A: Characteristics of Magnetic Disconnection Events Associated With SMM CMEs

[79] We have been involved in studies to characterize and evaluate the structural changes occurring in the corona during and following CMEs. In an earlier study, *Webb and Cliver* [1995] described results of an examination of some spaceborne coronagraph and ground-based solar

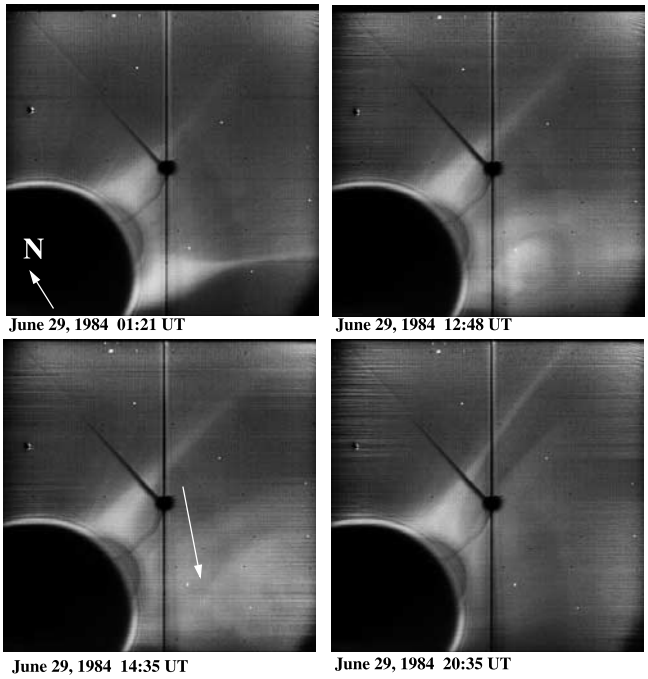


**Figure A1.** Example of a streamer blowout CME on 29 June 1984, with a large-scale concave-outward CDE at its base and, later, the evacuated corona. Time runs from upper left to lower right. The top left panel shows the preexisting streamer.

eclipse observations, searching for candidate disconnection events (CDEs) following CMEs. They examined images from total eclipses over the last 100 years, and coronagraph CME data sets for Skylab in 1973–1974 and SMM in 1980. Their results suggested that transient coronal structures similar to the prototypical *Illing and Hundhausen* [1983] event could be detected in the corona following about 10% of all CMEs. The average leading edge speed and width of these CMEs were less than those of typical CMEs, and the CDE features tended to be slower, narrower and fainter than their accompanying CMEs.

[80] Here we summarize the results of a second, following study: a comprehensive survey and analysis of CME CDEs observed by the HAO SMM coronagraph during the 5.5 years following the SMM repair between June 1984 and November 1989. This period was chosen because it provided a long period of continuous views of the lower corona ($<6\ R_S$) with a uniform data cadence, and a sufficient number of images to allow at least one complete view of the corona every 95 min. In addition, occasional views of the low corona ($1.2–2.2\ R_S$) were available from Mauna Loa Solar Observatory. *Webb and Burkepile* [1998] gave a preliminary report on results of the analysis of some key characteristics of the CDEs, however, the final results were never published. Because these SMM CDEs form the original data set from which the rays of the main paper were selected and for comparison with the earlier CDE studies, we present a summary of the analysis results of the SMM CMEs having CDEs in this Appendix.

[81] We selected the CMEs with optimal observations for detailed analysis from the catalog of *Burkepile and St. Cyr* [1993]. This catalog notes several features during CMEs of interest here that were called Concave-Outward or Lightbulb, or had outward-moving structures that were V-shaped or U-shaped. The CMEs we selected satisfied the following criteria: (1) at least one broadband image per orbit (every 90 min) of the appropriate sector or limb during the CME and for a duration of several consecutive orbits up to about 1 day afterward; (2) at least one good preevent image; (3) the image electronic artifacts did not obscure the CME or the structures trailing it; and (4) periods with extended data gaps of two or more orbits were avoided. We did not examine all the 1989 data in detail because the images were often degraded due to corongraph electronics and vidicon detector problems.

[82] We found ~60 CME/CDE events observed from 1984 to mid-November 1989. We examined each event in detail using the imaging displays at HAO. The CMEs associated with each CDE and the CDE itself were classified and the disconnection structures and any reforming streamers were analyzed. We measured the basic physical characteristics of the CDEs, including the morphology, speeds and widths of both the CDEs and their accompanying CMEs. We also studied the evidence for any newly formed rays and/or streamer structures and their locations and timing with regard to the preexisting streamer locations and CME and disconnection structures.

[83] An example of one of the SMM CMEs and CDEs is shown in Figure A1. It shows an example of a streamer blowout CME on 29 June 1984, with a large-scale, concave-outward CDE at its base, and later the evacuated corona. This is an example of a Webb and Cliver "class 1" CDE, i.e., a complete circular structure including the front of a CME. This event was not followed by a bright, transient ray.

[84] The final list of the 59 SMM CMEs which had CDEs is available from the first author, DFW. It is not presented here because of its length. Table A1 summarizes the rates of occurrence of the CMEs and disconnection events in this study, showing that, on average, about 10% of the SMM CMEs during this period had evidence of disconnection structures. There was a slight tendency for such structures to be more common during solar minimum in 1984–1986, suggesting that they may be more visible then due to the simpler nature of the background coronal structure.

[85] Mean values of the annual widths and speeds of the disconnection structures and their associated CMEs are given in Tables A2 and A3, respectively, by year and as total means. The mean value of the widths for all the data is 21°. The widths of the disconnection structures did not change much from solar cycle minimum to maximum. The mean value of the speeds for all the data is 138 km $s^{-1}$. The

**Table A1.** Annual Occurrence Rates of SMM CMEs and CDEs

| | Number of CMEs | Number of CDEs | Percent CDEs/CMEs |
|---|---|---|---|
| 1984 | 62 | 12 | 19.4 |
| 1985 | 57 | 7 | 12.3 |
| 1986 | 60 | 11 | 18.3 |
| 1987 | 117 | 9 | 7.7 |
| 1988 | 379 | 39 | 10.3 |
| 1989 | 507 | 46 | 9.1 |
| **Total** | **1182** | **124** | **10.5** |

**Table A2.** Annual Mean Widths of SMM CDEs and Associated CMEs

| | CDEs | | CMEs | |
|---|---|---|---|---|
| | Width, deg | Number of Events | Width, deg | Number of Events |
| 1984 | 23.4 | 8 | 33.9 | 8 |
| 1985 | 18.25 | 4 | 52.0 | 4 |
| 1986 | 22.3 | 7 | 35.5 | 8 |
| 1987 | 21.0 | 6 | 40.7 | 6 |
| 1988 | 22.6 | 21 | 51.1 | 17 |
| 1989 | 16.3 | 9 | 53.0 | 7 |
| **Total** | **21.2** | **55** | **44.9** | **50** |
| **Range** | **5–75** | | **7–108** | |

**Table A3.** Annual Mean Speeds of SMM CDEs and Associated CMEs

| | CDEs | | CMEs | |
|---|---|---|---|---|
| | Speed, km $s^{-1}$ | Number of Events | Speed, km $s^{-1}$ | Number of Events |
| 1984 | 67.9 | 7 | 185.8 | 6 |
| 1985 | 71.0 | 2 | | 0 |
| 1986 | 175.75 | 4 | 273.75 | 4 |
| 1987 | 125.4 | 5 | 172.0 | 4 |
| 1988 | 163.3 | 16 | 305.7 | 14 |
| 1989 | 173.25 | 4 | 731.5 | 4 |
| **Total** | **138.2** | **38** | **315.75** | **32** |
| **Range** | **29–435** | | **16–1956** | |

speeds of the disconnection structures did show changes over this same period, with a tendency for events at solar minimum to move more slowly.

[86] We studied the shapes of the CDEs, the effect of the CME on any associated streamer, and the existence of late transient rays for the 59 CDEs examined in detail. We found that the most common shape of the CDEs was U-shaped (20 of 59; 34%), with similar, lower rates for V-shaped (20%), lightbulb-shaped (19%), and questionable (27%). Just over half of the preexisting streamers associated with the CMEs were significantly disrupted, with 36% blown out or destroyed, and 25% disrupted. In 39% of the cases there was no apparent change or we could not tell. There was sufficient SMM data coverage and/or quality within ~12 hours of the CME onset to permit a search for later, transient rays for 45 of the 59 CDEs. About half of them (21 of 45, 47%) had bright, narrow rays following the CME/CDE in this time period. In an additional seven (16%) there was possibly a ray, and in the remaining 17 (38%) there was no visible late ray.

[87] Figure A2 is a histogram that compares the distributions of the widths of the CDEs and their associated CMEs. The mean of the CDE widths was 21° with a range of 5°–75°. The associated CMEs were about twice as wide, with a mean of 45° and a range of 7°–108°. This latter distribution is similar to the mean widths of all SMM CMEs (47° [*Hundhausen*, 1993]) and the median width of all LASCO CMEs (50° [*St. Cyr et al.*, 2000]).

[88] Figure A3 is a histogram that compares the distributions of the speeds of the CDEs and the speeds of the leading edge or cavity top of their associated CMEs. Where possible we derived the speeds of the CDE by measuring height/times of the lowest point of a concave-out feature or the vertex of a V-shaped feature. Most of the CDEs were slow, with a mean of 138 km $s^{-1}$ and a range of 29–435 km $s^{-1}$. Once again the associated CME speeds were more than twice as fast, with a mean of 316 km $s^{-1}$ and a range of 16–1956 km $s^{-1}$. The distribution of the associated CME speeds was very flat, with most of the speeds slower than the mean which is skewed by a few high-speed CMEs. This distribution is similar to that of all SMM CMEs (349 km $s^{-1}$), shown in the bottom panel from *Hundhausen et al.* [1994]. However, if only the speeds of the "outer loops" of SMM CMEs are included, the mean speed rises to 445 km $s^{-1}$. Such a radial speed gradient between the leading edge of a CME and material toward its base is typical of CME kinematics. The leading edge material is fastest and the trailing material progressively slower, like self-similar expansion [e.g., *Webb and Jackson*, 1981].

[89] In summary, we performed a comprehensive survey and analysis of CDEs trailing the main part of CMEs observed by the SMM coronagraph from 1984 through 1989. We found about 60 CMEs during this period which had CDEs, yielding an average rate of occurrence of CDEs of 10% of all SMM CMEs, in agreement with the prior results of *Webb and Cliver* [1995]. However, this rate was based on use of data from the older Skylab and SMM coronagraphs. With the more sensitive SOHO LASCO coronagraphs, *St. Cyr et al.* [2000] recently found that 36%, and possibly as high as 48% of LASCO CMEs exhibit a later concave-outward feature. Considering that subtle

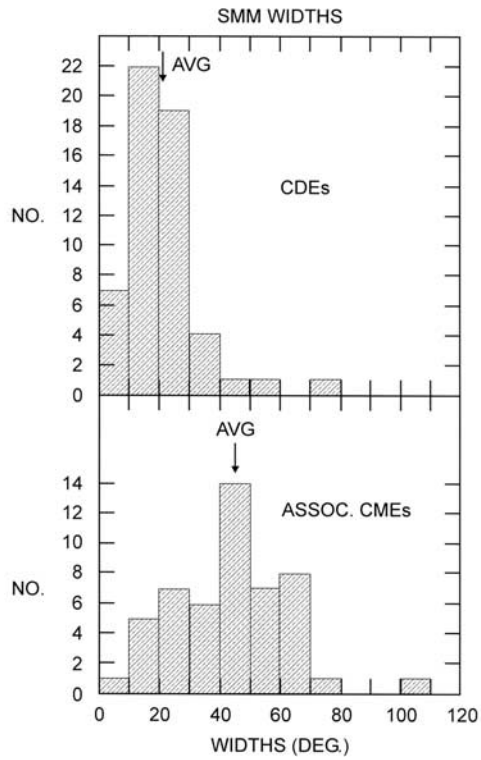


**Figure A2.** Histograms of the distributions of the widths of (top) the CDEs and (bottom) their associated CMEs in 10° bins. The average values of the widths are shown by the arrows.

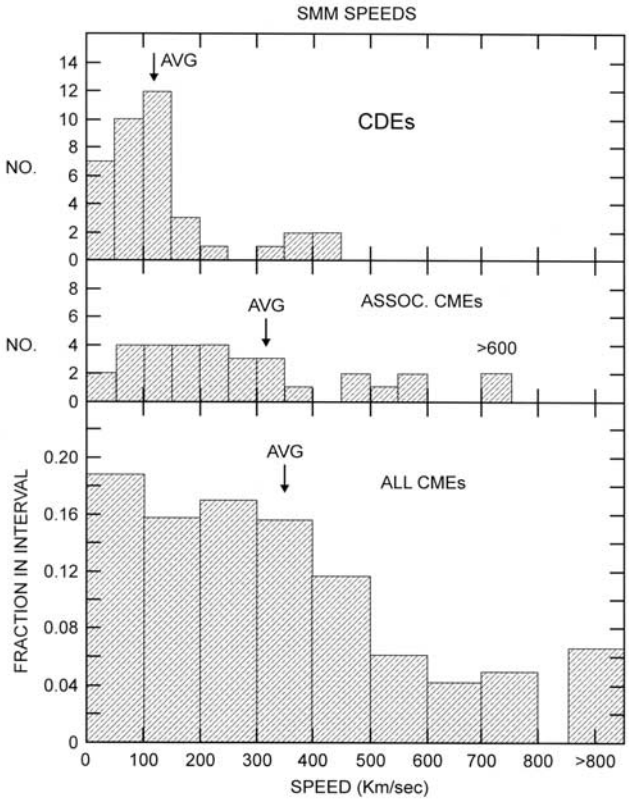


**Figure A3.** Histograms of the distributions of (top) the speeds of the CDEs and (middle) the speeds of the leading edge or cavity top of their associated CMEs in 50 km $s^{-1}$ bins. The distribution of the associated CME speeds was very flat, with most of the speeds slower than the mean which is skewed by a few high-speed CMEs. This distribution is similar to (bottom) that of all SMM CMEs, from *Hundhausen et al.* [1994].

CDE features may only be detectable for CMEs near the limb, this suggests the possibility that most CMEs contain such structures. This, in turn, suggests that reconnection/disconnection may be fundamental to the development of CMEs, although it is possible that such flux-rope-like structures form below the occulting disk, <2 $R_S$.

[90] We measured the morphology, speeds and widths of both the CDEs and their accompanying CMEs. The most common shape of the SMM CDEs was U-shaped. Just over half of the preexisting streamers associated with the CMEs were significantly disrupted, with 1/3 of these completely blown out or destroyed. About half of the CME/CDEs with adequate data coverage were followed within about 12 hours by bright, narrow, transient rays. This subset of the SMM/CDEs provided the basic data set for the study in the main paper. The mean width of the CDE structures was 21°. The associated CMEs were about twice as wide, with a mean width of 45°, similar to the mean widths of all SMM CMEs and the median width of all LASCO CMEs. Most of the CDEs were slow, with a mean speed of 138 km $s^{-1}$. The speeds of the associated CMEs were more than twice as fast, with a mean of 316 km $s^{-1}$. However, these CME speeds were less than those of all SMM CMEs, and significantly slower than the speeds of just the outer loops of SMM CMEs. The results of this study generally confirmed but extended the basic results of previous studies of CDEs, especially the *Webb and Cliver* [1995] study.

[91] **Acknowledgments.** Part of this work was done at HAO where DFW was supported by the National Center for Atmospheric Research (NCAR) Visiting Scientists appointments. NCAR is sponsored by the National Science Foundation. We thank A. Hundhausen of HAO, J. Raymond of the Center for Astrophysics, G. Lawrence of NRL, J. Linker of SAIC, and E. Cliver of AFRL for providing data or for helpful discussions involving this work. All of the authors have benefitted from their participation in the annual SHINE Workshops. This work was supported as follows: DFW by NASA grant NAG5-4946 and by Air Force contracts AF19628-96-K-0030 and AF19628-00-C-0073; TGF by NASA grants NAG5-8228 and NAG5-10977 to the University of New Hampshire, NAG5-10852 to Helio Research, and DoD MURI grants to the University of California at Berkeley and to the University of Michigan; PR by NSF SHINE grant ATM-0203817, NASA LWS grant NASW-02027, and the Center for Integrated Space Weather Modeling.

[92] Shadia Rifai Habbal thanks Volker Bothmer and another referee for their assistance in evaluating this paper.

## References

Amari, T., J. F. Luciani, Z. Mikic, and J. Linker, A twisted flux rope model for coronal mass ejections and two-ribbon flares, *Astrophys. J.*, *529*, L49, 2000.

Antiochos, S. K., C. R. DeVore, and J. A. Klimchuk, A model for solar coronal mass ejections, *Astrophys. J.*, *510*, 485, 1999.

Anzer, U., and A. I. Poland, Mass flow in loop type coronal transients, *Sol. Phys.*, *61*, 95, 1979.

Bastian, T. S., M. Pick, A. Kerdraon, D. Maia, and A. Vourlidas, The coronal mass ejection of 1998 April 20: Direct imaging at radio wavelengths, *Astrophys. J.*, *558*, L65, 2001.

Borrini, G., J. T. Gosling, S. J. Bame, W. C. Feldman, and J. M. Wilcox, Solar wind helium and hydrogen structure near the heliospheric current sheet: A signal of coronal streamers at 1 AU, *J. Geophys. Res.*, *86*, 4565, 1981.

Bothmer, V., Magnetic field structure and topology within CMEs in the solar wind, in *Solar Wind Nine*, edited by S. R. Habba et al., *AIP Conf. Proc.*, 471, 119, 1999.

Bothmer, V., and D. M. Rust, The field configuration of magnetic clouds and the solar cycle, in *Coronal Mass Ejections*, *Geophys. Monogr. Ser.*, vol. 99, edited by N. Crooker, J. A. Joselyn, and J. Feynman, p. 139, AGU, Washington, D. C., 1997.

Bothmer, V., and R. Schwenn, in *Mass Supply and Flows in the Solar Corona*, edited by B. Fleck, G. Noci, and G. Poletto, p. 225, Kluwer Acad., Norwell, Mass., 1994.

Burkepile, J. T., and O. C. St. Cyr, A revised and expanded catalogue of mass ejections observed by the solar maximum mission coronagraph, *Rep. NCAR/TN-369+STR*, Natl. Cent. for Atmos. Res., Boulder, Colo., 1993.

Cargill, P. J., and J. M. Schmidt, Modelling interplanetary CMEs using magnetohydrodynamic simulations, *Ann. Geophys.*, *20*, 879, 2002.

Chen, J., Effects of toroidal forces in current loops embedded in a background plasma, *Astrophys. J.*, *338*, 453, 1989.

Chen, J., et al., Evidence of an erupting magnetic flux rope: LASCO coronal mass ejection of 1997 April 13, *Astrophys. J.*, *490*, L91, 1997.

Chen, J., et al., Magnetic geometry and dynamics of the fast CME of 1997 September 9, *Astrophys. J.*, *533*, 481, 2000.

Chen, P. F., and K. Shibata, An emerging flux trigger mechanism for coronal mass ejections, *Astrophys. J.*, *545*, 524, 2000.

Ciaravella, A., J. C. Raymond, J. Li, P. Reiser, L. D. Gardner, Y. K. Ko, and S. Fineschi, Elemental abundances and post-coronal mass ejection current sheet in a very hot active region, *Astrophys. J.*, *575*, 1116, 2002.

Cliver, E. W., and H. S. Hudson, CMEs: How do the puzzle pieces fit together?, *J. Atmos. Sol. Terr. Phys.*, *64*, 231, 2002.

Cliver, E. W., et al., Solar gradual hard x-ray bursts and associated phenomena, *Astrophys. J.*, *305*, 920, 1986.

Crooker, N. U., Solar and heliospheric geoeffective disturbances, *J. Atmos. Sol. Terr. Phys.*, *62*, 1071, 2000.

Dere, K. P., G. E. Brueckner, R. A. Howard, D. J. Michels, and J. P. Delaboudiniere, LASCO and EIT observations of helical structre in coronal mass ejections, *Astrophys. J.*, *516*, 465, 1999.

Dryer, M., Coronal transient phenomena, *Space Sci. Rev.*, *33*, 233, 1982.

Fisher, R. R., and R. H. Munro, Coronal transient geometry. I. The flare-associated event of 1981 March 25, *Astrophys. J.*, *280*, 428, 1984.

Forbes, T. G., Numerical simulation of a catastrophe model for coronal mass ejections, *J. Geophys. Res.*, *95*, 11,919, 1990.

Forbes, T. G., A review on the genesis of coronal mass ejections, *J. Geophys. Res.*, *105*, 23,153, 2000.
Forbes, T. G., and L. W. Acton, Reconnection and field line shrinkage in solar flares, *Astrophys. J.*, *459*, 330, 1996.
Forbes, T. G., and P. A. Isenberg, A catastrophe mechanism for coronal mass ejection, *Astrophys. J.*, *373*, 294, 1991.
Forbes, T. G., and J. Lin, What can we learn about reconnection from coronal mass ejections?, *J. Atmos. Sol. Terr. Phys.*, *62*, 1499, 2000.
Forbes, T. G., and E. R. Priest, Photospheric magnetic field evolution and eruptive flares, *Astrophys. J.*, *446*, 377, 1995.
Forbes, T. G., J. M. Malherbe, and E. R. Priest, The formation of flare loops by magnetic reconnection and chromospheric ablation, *Sol. Phys.*, *120*, 285, 1989.
Forbes, T. G., E. R. Priest, and P. A. Isenberg, On the maximum energy release in flux-rope models of eruptive flares, *Sol. Phys.*, *150*, 245, 1994.
Gibson, S. E., and B. C. Low, A time-dependent three-dimensional magnetohydrodynamic model of coronal mass ejections, *Astophys. J.*, *493*, 360, 1998.
Gold, T., Magnetic storms, *Space Sci. Rev.*, *1*, 100, 1962.
Gopalswamy, N., M. R. Kundu, P. K. Manoharan, A. Raoult, N. Nitta, and P. Zarka, X-ray and radio studies of a coronal eruption: Shock wave, plasmoid, and coronal mass ejection, *Astrophys. J.*, *486*, 1036, 1997.
Gosling, J. T., Large-scale inhomogeneities in the solar wind of solar origin, *Rev. Geophys.*, *13*, 1053, 1975.
Gosling, J. T., The solar flare myth, *J. Geophys. Res.*, *98*, 18,937, 1993.
Gosling, J. T., E. Hildner, R. M. MacQueen, R. H. Munro, A. I. Poland, and C. L. Ross, Mass ejections from the Sun: A view from Skylab, *J. Geophys. Res.*, *79*, 4581, 1974.
Gosling, J. T., J. Birn, and M. Hesse, Three-dimensional magnetic reconnection and the magnetic topology of coronal mass ejection events, *Geophys. Res. Lett.*, *22*, 869, 1995.
Harrison, R. A., Solar coronal mass ejections and flares, *Astron. Astrophys.*, *162*, 283, 1986.
Harrison, R. A., and M. Lyons, A spectroscopic study of coronal dimming associated with a coronal mass ejection, *Astron. Astrophys.*, *358*, 1097, 2000.
Hiei, E., A. J. Hundhausen, and D. G. Sime, Reformation of a coronal helmet streamer by magnetic reconnection after a coronal mass ejection, *Geophys. Res. Lett.*, *20*, 2785, 1993.
Hildner, E., Mass ejections from the solar corona into interplanetary space, in *Study of Traveling Interplanetary Phenomena*, edited by M. Shea, p. 3, D. Reidel, Norwell, Mass., 1977.
Hudson, H. S., and J. I. Khan, Observational problems for flare models based on large-scale magnetic reconnection, in *Magnetic Reconnection in the Solar Atmosphere*, *ASP Conf. Ser.*, vol. 111, edited by R. Bentley and J. T. Mriska, p. 135, Astron. Soc. of the Pac., San Francisco, Calif., 1996.
Hudson, H. S., and D. F. Webb, Soft X-ray signatures of coronal ejections, in *Coronal Mass Ejections*, *Geophys. Monogr. Ser.*, vol. 99, edited by N. Crooker, J. A. Joselyn, and J. Feynman, p. 27, AGU, Washington, D. C., 1997.
Hudson, H. S., J. R. Lemen, and D. F. Webb, Coronal dimming in two limb flares, in *Magnetic Reconnection in the Solar Atmosphere*, *ASP Conf. Ser.*, vol. 111, edited by R. Bentley, and J. T. Mriska, p. 379, Astron. Soc. of the Pac., San Francisco, Calif., 1996.
Hudson, H. S., J. R. Lemen, O. C. St. Cyr, A. C. Sterling, and D. F. Webb, X-ray coronal changes during halo CMEs, *Geophys. Res. Lett.*, *25*, 2481, 1998.
Hundhausen, A. J., An interplanetary view of coronal holes, in *Coronal Holes and High Speed Wind Streams*, edited by J. B. Zirker. p. 225, Colo. Assoc. Univ. Press, Boulder, 1977.
Hundhausen, A. J., Sizes and locations of coronal mass ejections: SMM observations from 1980 and 1984–1989, *J. Geophys. Res.*, *98*, 13,177, 1993.
Hundhausen, A. J., Coronal mass ejections: A summary of SMM observations from 1980 and 1984–1989, in *The Many Faces of the Sun*, edited by K. Strong et al., p. 143, Springer-Verlag, New York, 1999.
Hundhausen, A. J., J. T. Burkepile, and O. C. St. Cyr, Speeds of coronal mass ejections: SMM observations from 1980 and 1984–1989, *J. Geophys. Res.*, *99*, 6543, 1994.
Illing, R. M. E., and A. J. Hundhausen, Possible observation of a disconnected magnetic structure in a coronal transient, *J. Geophys. Res.*, *88*, 10,210, 1983.
Kahler, S. W., and H. S. Hudson, Origin and development of transient coronal holes, *J. Geophys. Res.*, *106*, 29,239, 2001.
Kahler, S. W., and A. J. Hundhausen, The magnetic topology of solar coronal structures following mass ejections, *J. Geophys. Res.*, *97*, 1619, 1992.
Kahler, S. W., and D. V. Reames, Probing the magnetic topologies of magnetic clouds by means of solar energetic particles, *J. Geophys. Res.*, *96*, 9419, 1991.
Klimchuk, J. A., Theory of coronal mass ejections, in *Space Weather*, *Geophys. Monogr. Ser.*, vol. 125, edited by P. Song, H. J. Singer, and G. L. Siscoe, p. 143, AGU, Washington, D. C., 2001.
Ko, Y., J. C. Raymond, J. Lin, G. Lawrence, J. Li, and A. Fludra, Dynamical and physical properties of a post-CME current sheet, *Astrophys. J.*, *594*, 1068–1084, 2003.
Lin, J., Energetics and propagation of coronal mass ejections in different plasma environments, *Chin. J. Astron. Astrophys.*, *2*, 539, 2002.
Lin, J., and T. G. Forbes, Effects of reconnection on the coronal mass ejection process, *J. Geophys. Res.*, *105*, 2375, 2000.
Lin, J., T. G. Forbes, E. R. Priest, and T. N. Bungey, Models for the motions of flare loops and ribbons, *Sol. Phys.*, *159*, 275, 1995.
Lin, J., T. G. Forbes, P. A. Isenberg, and P. D. Moulin, The effect of curvature on flux-rope models of coronal mass ejections, *Astrophys. J.*, *504*, 1006, 1998.
Linker, J. A., R. Lionello, Z. Mikic, and T. Amari, Magnetohydrodynamic modeling of prominence formation within a helmet streamer, *J. Geophys. Res.*, *106*, 25,165, 2001.
Linker, J. A., Z. Mikic, R. Lionello, P. Riley, T. Amari, and D. Odstrcil, Flux cancellation and coronal mass ejections, *Phys. Plasmas*, *10*, 1971, 2003.
Low, B. C., Eruptive solar magnetic fields, *Astrophys. J.*, *251*, 352, 1981.
Low, B. C., On the large-scale magnetostatic coronal structures and their stability, *Astrophys. J.*, *286*, 772, 1984.
Low, B. C., Equilibrium and dynamics of coronal magnetic fields, *Annu. Rev. Astron. Astrophys.*, *28*, 491, 1990.
Low, B. C., Coronal mass ejections, flares and prominences, in *Solar Wind Nine*, edited by S. R. Habbal et al., p. 109, Am. Inst. of Phys., Woodbury, N. Y., 1999.
Low, B. C., and D. F. Smith, The free energies of partially open magnetic fields, *Astrophys. J.*, *410*, 412, 1993.
MacQueen, R. M., Coronal transients: A summary, *Philos. Trans. R. Soc. London, Ser. A*, *297*, 605, 1980.
MacQueen, R. M., and O. C. St. Cyr, Sungrazing comets observed by the Solar Maximum Mission corongraph, *Icarus*, *90*, 96, 1991.
MacQueen, R. M., A. J. Hundhausen, and C. W. Conover, The propagation of coronal mass ejection transients, *J. Geophys. Res.*, *91*, 31, 1986.
Magara, T., S. Mineshige, T. Yokoyama, and K. Shibata, Numerical simulation of magnetic reconnection in eruptive flares, *Astrophys. J.*, *466*, 1054, 1996.
Magara, T., K. Shibata, and T. Yokoyama, Evolution of eruptive flares. I. Plasmoid dynamics in eruptive flares, *Astrophys. J.*, *487*, 437, 1997.
Mann, G., A. Klassen, H. Aurass, and H. T. Classen, Formation and development of shock waves in the solar corona and the near-Sun interplanetary space, *Astron. Astrophys.*, in press, 2003.
Martens, P. C. H., and N. P. M. Kuin, A circuit model for filament eruptions and two-ribbon flares, *Sol. Phys.*, *122*, 263, 1989.
Marubashi, K., Physics of interplanetary magnetic flux ropes: Toward prediction of geomagnetic storms, *Adv. Space Res.*, *26*(1), 55, 2000.
McComas, D. J., Tongues, bottles, and disconnected loops: The opening and closing of the interplanetary magnetic field, *Rev. Geophys.*, *33*, 603, 1995.
McComas, D. J., J. T. Gosling, and J. L. Phillips, Interplanetary magnetic flux: Measurement and balance, *J. Geophys. Res.*, *97*, 171, 1992.
McKenzie, D. E., Supra-arcade downflows in long-duration solar flare events, *Sol. Phys.*, *195*, 381, 2000.
McKenzie, D. E., and H. S. Hudson, X-ray observations of motions and structure above a solar flare arcade, *Astrophys. J.*, *519*, L93, 1999.
Mikic, Z., and J. A. Linker, Disruption of coronal magnetic field arcades, *Astrophys. J.*, *430*, 898, 1994.
Mikic, Z., and J. A. Linker, The initiation of coronal mass ejections by magnetic shear, in *Coronal Mass Ejections*, *Geophys. Monogr. Ser.*, vol. 99, edited by N. Crooker, J. A. Joselyn, and J. Feynman, p. 57, AGU, Washington, D. C., 1997.
Moore, R. L., and G. Roumeliotis, Triggering of eruptive flares—Destabilization of the preflare magnetic field configuration, in *Eruptive Solar Flares*, edited by Z. Svestka, B. V. Jackson, and M. E. Machado, p. 69, Springer-Verlag, New York, 1992.
Moore, R. L., et al., The thermal X-ray flare plasma, in *Solar Flares*, edited by P. A. Sturrock, p. 341, Colo. Assoc. Univ. Press, Boulder, 1980.
Neugebauer, M., R. Goldstein, and B. E. Goldstein, Features observed in the trailing regions of interplanetary clouds from coronal mass ejections, *J. Geophys. Res.*, *102*, 19,743, 1997.
Nitta, N., and S. Akiyama, Relation between flare-associated X-ray ejections and coronal mass ejections, *Astophys. J.*, *525*, L57, 1999.
Odstrcil, D., J. A. Linker, R. Lionello, Z. Mikic, P. Riley, V. J. Pizzo, and J. G. Luhmann, Merging of coronal and heliopsheric numerical two-dimensional MHD models, *J. Geophys. Res.*, *107*(A12), 1493, doi:10.1029/2002JA009334, 2002.

Parker, E. N., Sweet's mechanism for merging magnetic fields in conducting fluids, *J. Geophys. Res.*, *62*, 509, 1957.
Parker, E. N., The dynamical properties of twisted ropes of magnetic field and the vigor of new active regions on the Sun, *Astrophys. J.*, *191*, 245, 1974.
Plunkett, S. P., Simultaneous SOHO and ground-based observations of a large eruptive prominence and coronal mass ejection, *Sol. Phys.*, *94*, 371, 2000.
Poletto, G., and R. A. Kopp, Macroscopic electric fields during two-ribbon flares, in *The Lower Atmosphere of Solar Flares*, edited by D. F. Neidig, p. 453, Natl. Sol. Obs., Sunspot, N. M., 1986.
Priest, E. R., and T. G. Forbes, *Magnetic Reconnection—MHD Theory and Applications*, Cambridge Univ. Press, New York, 2000.
Riley, P., J. A. Linker, Z. Mikic, D. Odstrcil, V. J. Pizzo, and D. F. Webb, Evidence of post-eruption reconnection associated with coronal mass ejections in the solar wind, *Astrophys. J.*, *578*, 972, 2002.
Riley, P., J. A. Linker, Z. Miki, D. Odstrcil, T. H. Zurbuchen, D. Lario, and R. P. Lepping, Using an MHD simulation to interpret the global context of a coronal mass ejection observed by two spacecraft, *J. Geophys. Res.*, *108*(A7), 1272, doi:10.1029/2002JA009760, 2003.
Roussev, I. I., T. G. Forbes, T. Gombosi, and I. Sokolov, Numerical test of a three-dimensional flux rope model for coronal mass ejections based on ideal MHD processes, *Eos Trans. AGU*, *83*(47), Fall Meet. Suppl., Abstract SH21A-0476, 2002.
Rust, D. M., Coronal disturbances and their terrestrial effects, *Space Sci. Rev.*, *34*, 21, 1983.
Rust, D. M., Spawning and shedding helical magnetic fields in the solar atmosphere, *Geophys. Res. Lett.*, *21*, 241, 1994.
Shafranov, V. D., Plasma equilibrium in a magnetic field, *Rev. Plasma Phys.*, *2*, 103, 1966.
Sheeley, N. R., Jr., R. A. Howard, M. J. Koomen, and D. J. Michels, Associations between coronal mass ejections and soft X-ray events, *Astrophys. J.*, *272*, 349, 1983.
Shibata, K., et al., Hot-plasma ejections associated with compact-loop solar flares, *Astrophys. J.*, *451*, L83, 1995.
Shodhan, S., N. U. Crooker, S. W. Kahler, R. J. Fitzenreiter, D. E. Larson, R. P. Lepping, G. L. Siscoe, and J. T. Gosling, Counterstreaming electrons in magnetic clouds, *J. Geophys. Res.*, *105*, 27,261, 2000.
Simnett, G. M., et al., LASCO observations of disconnected magentic structures out to beyond 28 solar radii during coronal mass ejections, *Sol. Phys.*, *175*, 685, 1997.
Sittler, E. C. J., and M. Guhathakurta, Semiempirical two-dimensional magnetohydrodynamics model of the solar corona and interplanetary medium, *Astrophys. J.*, *523*, 812, 1999.
St. Cyr, O. C., et al., Properties of coronal mass ejections: SOHO LASCO observations from January 1996 to June 1998, *J. Geophys. Res.*, *105*, 18,169, 2000.
Steinolfson, R. S., and A. J. Hundhausen, Density and white light brightness in looplike coronal mass ejections: Temporal evolution, *J. Geophys. Res.*, *93*, 14,269, 1988.
Sturrock, P. A., The role of eruption in solar flares, *Sol. Phys.*, *121*, 387, 1989.
Sturrock, P. A., M. Weber, M. S. Wheatland, and R. Wolfson, Metastable magnetic configurations and their significance for solar eruptive events, *Astrophys. J.*, *548*, 492, 2001.
Svestka, Z., and E. W. Cliver, History and basic characteristics of eruptive flares, in *Eruptive Solar Flares*, edited by Z. Svestka, B. Jackson, and M. Machado, p. 1, Springer-Verlag, New York, 1992.
Svestka, Z., J. M. Fontenla, M. E. Machado, S. F. Martin, D. F. Neidig, and G. Poletto, Multithermal observations of newly formed loops in a dynamic flare, *Sol. Phys.*, *108*, 237, 1987.
Thompson, B. J., E. W. Cliver, N. Nitta, C. Delannée, and J. P. Delaboudiniére, Coronal dimmings and energetic CMEs in April–May 1998, *Geophys. Res. Lett.*, *27*, 1431, 2000.
Tsuneta, S., S. Masuda, T. Kosugi, and J. Sato, Hot and superhot plasmas above an impulsive flare loop, *Astrophys. J.*, *478*, 787, 1997.
van Ballegooijen, A. A., and P. C. H. Martens, Formation and eruption of solar prominences, *Astrophys. J.*, *343*, 971, 1989.
van Tend, W., and M. Kuperus, The development of coronal electric current systems in active regions and their relation to filaments and flares, *Sol. Phys.*, *59*, 115, 1978.
Wagner, W. J., E. Hildner, L. L. House, C. Sawyer, K. V. Sheridan, and G. A. Dulk, Radio and visible light observations of matter ejected from the Sun, *Astrophys. J.*, *244*, L123, 1981.
Wang, A. H., S. T. Wu, S. T. Suess, and G. Poletto, Global model of the corona with heat and momentum addition, *J. Geophys. Res.*, *103*, 1913, 1998a.
Wang, Y. M., et al., Origin of streamer material in the outer corona, *Astrophys. J.*, *498*, L165, 1998b.
Webb, D. F., Erupting prominences and the geometry of coronal mass ejections, *J. Geophys. Res.*, *93*, 1749, 1988.
Webb, D. F., CMEs and the solar cycle variation in their geoeffectivenss, in *Proceedings of the SOHO 11 Symposium, From Solar Min to Max: Half a Solar Cycle With SOHO*, *Rep. ESA SP-508*, p. 409, Eur. Space Res. and Technol. Cent., Noordwijk, Netherlands, 2002.
Webb, D. F., and J. Burkepile, Characteristics of magnetic disconnection events associated with SMM CMEs: 1984–89 (abstract), *Eos Trans AGU*, *79*(17), Spring Meet. Suppl., S257, 1998.
Webb, D. F., and E. W. Cliver, Evidence for magnetic disconnection of mass ejections in the corona, *J. Geophys. Res.*, *100*, 5853, 1995.
Webb, D. F., and B. V. Jackson, Kinematical analysis of spray ejecta observed in the corona, *Sol. Phys.*, *73*, 341, 1981.
Webb, D. F., J. Burkepile, and T. G. Forbes, Observational evidence of new current sheets following CMEs, *Eos Trans. AGU*, *82*(20), Spring Meet. Suppl., Abstract SH51C-03, 2001.
Wolfson, R., and B. Dlamini, Cross-field currents: An energy source for coronal mass ejections?, *Astrophys. J.*, *483*, 961, 1997.
Wood, B. E., M. Karovska, J. Chen, G. E. Brueckner, J. W. Cook, and R. A. Howard, Comparison of two coronal mass ejections observed by EIT and LASCO with a model of an erupting magnetic flux rope, *Astrophys. J.*, *512*, 484, 1999.
Wu, S. T., and W. P. Guo, A self-consistent numerical MHD model of helmet streamer and flux rope interactions: Initiation and propagation of coronal mass ejections (CMEs), in *Coronal Mass Ejections*, *Geophys. Monogr. Ser.*, vol. 99, edited by N. Crooker, J. A. Joselyn, and J. Feynman, p. 83, AGU, Washington, D. C., 1997.
Wu, S. T., W. P. Guo, and J. F. Wang, Dynamical evolution of a coronal streamer-bubble system, *I, Sol. Phys.*, *157*, 325, 1995.
Wu, S. T., et al., MHD interpretation of LASCO observations of a coronal mass ejection as a disconnected magnetic structure, *Sol. Phys.*, *175*, 719, 1997.
Wu, S. T., W. P. Guo, D. J. Michels, and L. F. Burlaga, MHD description of the dynamical relationships between a flux rope, streamer, coronal mass ejection, and magnetic cloud: An analysis of the January 1997 Sun-Earth connection event, *J. Geophys. Res.*, *104*, 14,789, 1999.
Wu, S. T., W. P. Guo, S. P. Plunkett, B. Schmieder, and G. M. Simnett, Coronal mass ejections (CMEs) initiation: Models and observations, *J. Atmos. Sol. Terr. Phys.*, *62*, 1489, 2000.
Wu, S. T., M. D. Andrews, and S. P. Plunkett, Numerical magnetohydrodynamic (MHD) modeling of coronal mass ejections (CMEs), *Space Sci. Rev.*, *95*, 191, 2001.
Yokoyama, T., K. Akita, T. Morimoto, K. Inoue, and J. Newmark, Clear evidence of reconnection inflow of a solar flare, *Astophys. J.*, *546*, L69, 2001.

J. Burkepile, High Altitude Observatory, National Center for Atmospheric Research, 3450 Mitchell Lane, Boulder, CO 80307, USA. (iguana@hao.ucar.edu)

T. G. Forbes, Space Science Center/Institute for the Study of Earth, Oceans, and Space, Morse Hall, University of New Hampshire, Durham, NH 03824, USA. (terry.forbes@unh.edu)

P. Riley, Science Applications International Corporation, 10620 Campus Point Drive, San Diego, CA 92121, USA. (pete.riley@saic.com)

D. F. Webb, AFRL/VSBXS, 29 Randolph Road, Hanscom AFB, MA 01731-3010, USA. (david.webb@hanscom.af.mil)